Vglut2-based glutamatergic signaling in central noradrenergic neurons is dispensable for normal breathing and chemosensory reflexes

Author names and affiliations

Yuan Chang[1,2], Savannah Lusk[1], Andersen Chang[1], Christopher S Ward[2], Russell S Ray[1,2,3,4]

[1]Department of Neuroscience, Baylor College of Medicine, Houston, TX, USA

[2]Department of Integrative Physiology, Baylor College of Medicine, Houston, TX, USA

[3]McNair Medical Institute, Houston, TX, USA

[4]Corresponding author, russell.ray@bcm.edu

Abstract

Central noradrenergic (NA) neurons are key constituents of the respiratory homeostatic network. NA dysfunction is implicated in several developmental respiratory disorders including Congenital Central Hyperventilation Syndrome (CCHS), Sudden Infant Death Syndrome (SIDS) and Rett Syndrome. The current unchallenged paradigm in the field, supported by multiple studies, is that glutamate co-transmission in subsets of central NA neurons plays a role in breathing control. If true, NA-glutamate co-transmission may also be mechanistically important in respiratory disorders. However, the requirement of NA-derived glutamate in breathing has not been directly tested and the extent of glutamate co-transmission in the central NA system remains uncharacterized. Therefore, we fully characterized the cumulative fate maps and acute adult expression patterns of all three Vesicular Glutamate Transporters (*Slc17a7* (Vglut1), *Slc17a6* (Vglut2), and *Slc17a8* (Vglut3)) in NA neurons, identifying a novel, dynamic expression pattern for Vglut2 and an undescribed co-expression domain for Vglut3 in the NA system. In contrast to our initial hypothesis that NA derived glutamate is required to breathing, our functional studies showed that loss of Vglut2 throughout the NA system failed to alter breathing or metabolism under room air, hypercapnia, or hypoxia in unrestrained and unanesthetized mice. These data demonstrate that Vglut2-based glutamatergic signaling within the central NA system is not required for normal baseline breathing and hypercapnic, hypoxic chemosensory reflexes. These

outcomes challenge the current understanding of central NA neurons in the control of breathing and suggests that glutamate may not be a critical target to understand NA neuron dysfunction in respiratory diseases.

Introduction

Breathing is a vital and life-sustaining function supporting homeostatic processes, most critically maintaining blood pH/CO_2 and O_2 levels within a narrow physiological range. Respiratory homeostasis is mediated by neuron-modulated lung ventilation adjustments in response to physiological deviations resulting in high pCO_2 or low pO_2 blood and tissue levels, known as the hypercapnic and hypoxic reflexes respectively (Del Negro et al., 2018; Dick et al., 2018). These reflexes are part of a complex brainstem neural network that integrates a multitude of information streams across the central and peripheral nervous systems to regulate respiratory output. Within this brainstem network, central noradrenergic (NA) neurons are known to be an important component that plays a variety of roles in modulating breathing. Furthermore, various perturbations across the central NA system have been implicated in several developmental disorders with respiratory and chemosensory features such as Congenital Central Hyperventilation Syndrome (CCHS), Sudden Infant Death Syndrome (SIDS) and Rett Syndrome (Beltrán-Castillo et al., 2017; Feldman et al., 2013; Gauda et al., 2007; Viemari, 2008). Thus, understanding how central NA neurons modulate respiratory chemoreflexes or chemosensory breathing is critically important for the development of new diagnostic and therapeutic interventions to address respiratory pathophysiology.

Central noradrenergic neurons are commonly thought to exert their effect on breathing through their primary neurotransmitter noradrenaline and adrenaline. However, in addition to noradrenaline, several studies provide strong evidence that glutamate is co-transmitted in subsets of central NA neurons. Vesicular glutamate transporter 2 (Vglut2), a gene marker of glutamatergic signaling, has been shown to be co-expressed in subsets of central NA neurons including, C1/A1, C2/A2, A5, and LC in adult rats and mice (DePuy et al., 2013; Souza et al., 2022a; Stornetta et al., 2002a, 2002b; Yang et al., 2021), though NA specific expression of

59 related Vglut1 and Vglut3 transporters remains unknown. Additionally, it has been well
60 documented that central NA neurons co-expressing Vglut2 innervate key respiratory centers,
61 such as preBötzinger complex and parafacial region (pFRG). Additionally, central NA neurons co-
62 expressing Vglut2 project to many key autonomic brainstem, spinal cord, and forebrain centers,
63 such as the dorsal motor nucleus of the vagus, intermediolateral nucleus (IML) and sympathetic
64 system, and the hypothalamus, all of which could drive a change in breathing if perturbed, i.e.,
65 indirect effects from cardio-vascular and metabolic dysregulation (Supplemental table 1). Thus,
66 it has become a dominant paradigm in the field of respiratory physiology that NA-based
67 glutamate release is a critical form of neurotransmission in the control of breathing. Abbott et al.
68 (2014) showed that Vglut2 is required for an increase in respiratory rate when anterior C1
69 neurons are unilaterally opto-genetically stimulated. Malheiros-Lima et al. (2020) showed that
70 Vglut2-expressing C1 neurons project to the pFRG region, and hypoxic breathing was blunted
71 after blockade of ionotropic glutamatergic receptors at the pFRG site in anesthetized rats,
72 together supporting a role for anterior C1 neurons releasing glutamate at the pFRG site to
73 regulate breathing under hypoxia. Similarly, Malheiros-Lima et al. (2022) and Malheiros-Lima et
74 al. (2018) showed that Vglut2-expressing C1 neurons project to the NA A5 region and the
75 preBötzinger complex, and, again, the blockade of ionotropic glutamatergic receptors at the A5
76 region or preBötzinger complex reduced the increase in phrenic nerve activity and respiratory
77 frequency elicited by optogenetic stimulation of C1 cells in an anesthetized preparation. In
78 addition, Guyenet et al. (2013) and others speculated that the apparent lack of plasmalemmal
79 monoamine transporter in C1 fibers indicates reduced or absent noradrenergic or adrenergic
80 signaling due a lack of re-uptake and neurotransmitter pool depletion (Comer et al., 1998; Lorang
81 et al., 1994). Cumulatively, the studies argue for glutamate as the predominant functional
82 neurotransmitter for C1 NA neurons in the breathing neural network. To our knowledge, this
83 dominant perspective has not been otherwise previously challenged. Although these studies are
84 informative, the evidence supporting the role of NA-based Vglut2 signaling in respiratory control
85 are either indirect and circumstantial or cannot be seen as physiological given experimental
86 limitations, such as the focal nature of opto-genetic stimulation. Thus, it is not yet clear what the

87 requirement is for NA-based glutamatergic signaling in homeostatic breathing in the
88 unanesthetized and unrestrained animal and how that might inform upon disease.
89
90 To better understand the role of NA-based glutamatergic signaling in breathing, we sought to
91 both fully characterize the molecular profiles of the central noradrenergic system with respect to
92 glutamate co-expression and to test the hypothesis that Vglut2-based glutamatergic release is
93 required in respiratory control under physiological chemosensory challenges in unanesthetized
94 and unrestrained mice. We first fully characterized the recombinase-based cumulative fate maps
95 for Vglut1, Vglut2 and Vglut3 expression and compared those maps to their real time expression
96 profiles in central NA neurons by RNA *in situ* hybridization in adult mice. We found a novel
97 dynamic expression pattern for Vglut2 and an entirely undescribed co-expression domain for
98 Vglut3 in the central NA system. Secondly, to determine if Vglut2-based glutamatergic signaling
99 in NA neurons is required for respiratory homeostasis, we conditionally ablated Vglut2 in all NA
100 neurons and tested respiratory, chemosensory, and metabolic function in unrestrained and
101 unanesthetized mice. Using the same genetic model in prior studies (Abbott et al., 2014),
102 conditional deletion of Vglut2 in NA neurons did not significantly impact breathing under room
103 air, hypercapnic, or hypoxic conditions. These results demonstrate, for the first time, that NA
104 Vglut2-based glutamatergic signaling is dispensable for respiratory control, which challenges the
105 prevalent perspective on the role of C1 and other Vglut2 expressing NA neurons in respiratory
106 homeostasis and suggests that glutamate may not be a critical target to understand NA neuron
107 dysfunction in respiratory diseases.
108
109 **Results**
110 **Cumulative fate maps of central noradrenergic neurons co-expressing Vglut1, Vglut2 and**
111 **Vglut3**
112 To fully characterize the expression profiles of all three glutamate markers Vglut1, Vglut2 and
113 Vglut3 in central noradrenergic neurons, we first used an intersectional genetic strategy (Figure
114 1A). We bred three Cre drivers *Slc17a7*^{Cre} (Vglut1-Cre), *Slc17a6*^{Cre} (Vglut2-Cre) and *Slc17a8*^{Cre}
115 (Vglut3-Cre) to *Dbh*$^{p2a\text{-}Flpo}$ (DBH-p2a-Flpo) (targeting noradrenergic neurons) mice, respectively.

116 The three compound lines of *Slc17a7*^{Cre}; *Dbh*$^{p2a\text{-}Flpo}$, *Slc17a6*^{Cre}; *Dbh*$^{p2a\text{-}Flpo}$, and *Slc17a8*^{Cre}; *Dbh*$^{p2a\text{-}}$
117 ^{Flpo} were then crossed with the *Rosa26*$^{RC::FLTG}$ (RC::FLTG). RC::FLTG are intersectional reporter
118 mice that express tdTomato in cells expressing only flippase (Flpo) and express eGFP in cells co-
119 expressing both Flpo and Cre recombinases. Thus, in each of the three intersectional reporter
120 crosses [e.g. 1) *Slc17a7*^{Cre}; *Dbh*$^{p2a\text{-}Flpo}$; *Rosa26*$^{RC::FLTG}$, 2) *Slc17a6*^{Cre}; *Dbh*$^{p2a\text{-}Flpo}$; *Rosa26*$^{RC::FLTG}$ and
121 3) *Slc17a8*^{Cre}; *Dbh*$^{p2a\text{-}Flpo}$; *Rosa26*$^{RC::FLTG}$], NA neurons without any Vglut1, 2, or 3 expression are
122 labelled by red fluorescent protein (tdTomato) while NA neurons co-expressing either Vglut1,
123 Vglut2, or Vglut3 are labeled by green fluorescent protein (eGFP). By using this method, we
124 characterized and quantified the expression profiles of all three vesicular glutamate transporters
125 Vglut1, Vglut2, and Vglut3 across every anatomically defined NA nucleus in adult mice including
126 A7, Locus Coeruleus (LC), dorsal/ ventral subcoeruleus nucleus (sub CD/CV), A5, and the anterior
127 - posterior dimensions of C1/A1, C2/A2 (Robertson et al., 2013), and C3 (Figure 1B-D and Figure
128 1 supplement 1A-B). Vglut1-Cre was not co-expressed in any central NA nuclei in adult mice.
129 However, Vglut2-Cre and Vglut3-Cre both showed co-expression in central NA neurons. Vglut3-
130 Cre-expressing NA neurons were restricted to posterior C2/A2 and posterior C1/A1, with greatest
131 expression in posterior C2/A2 where 26.9 $\pm$ 3.16% of NA neurons were Vglut3-Cre positive. In
132 posterior C1/A1, only 1.26 $\pm$ 0.559% of NA neurons were Vglut3-Cre positive. Surprisingly, 84.6 $\pm$
133 3.75% of NA neurons in total showed Vglut2-Cre co-expression and each NA nucleus was
134 predominantly labelled by Vglut2-Cre expression. Over 50% of NA neurons in each NA nucleus
135 were Vglut2-Cre positive. The percentages of Vglut2-Cre positive NA neurons in each NA nucleus
136 were as follows: 69.8 $\pm$ 8.29% in A7, 80.5 $\pm$ 3.78% in LC, 84.8 $\pm$ 11.3% in A5, 51.5 $\pm$ 2.61% in sub
137 CD/CV, 99.0 $\pm$ 0.681% in anterior C1/A1, 95.7 $\pm$ 2.40% in posterior C1/A1, 96.1 $\pm$ 1.98% in anterior
138 C2/A2, 97.8 $\pm$ 0.771% in posterior C2/A2, and 100 $\pm$ 0.00% in C3 (Mean $\pm$ SEM). The presence of
139 Vglut2-Cre co-expression in anterior NA groups was unexpected as previous *in situ* data in adult
140 rats found *Slc17a6* (Vglut2) positive NA neurons only in the posterior C2/A2 and C1/A1 (Stornetta
141 et al., 2002a, 2002b). Notably, however, the Vglut2 co-expression in the LC region agrees with
142 Yang et al. (2021) which also showed that 89% of LC NA neurons are Vglut2 positive using a
143 different intersectional strategy in mice: *Th*^{Flpo}*; Slc17a6*^{Cre}*; Rosa26*^{Ai65} (TH-Flpo; Vglut2-Cre; Ai65).
144 The differences in our and other fate maps compared to *in situ* hybridization may either reflect

145 early gene expression that is down regulated in the adult or may reflect low levels of expression
146 not detectable by *in situ* hybridization but that are nonetheless sufficient to affect recombination
147 in the intersectional genetic strategy.
148
149 **Real time mRNA expression patterns of Vglut1, Vglut2 and Vglut3 in central noradrenergic**
150 **neurons in adult mice**
151 To verify if the real time NA-based Vglut2 expression pattern in adult mice is comparable to
152 previous reports in adult rats (DePuy et al., 2013; Stornetta et al., 2002b, 2002a), and to further
153 characterize the expression patterns of the other two vesicular glutamate transporters (Vglut1
154 and Vglut3) in adult mice, we performed fluorescent RNA *in situ* hybridization experiments. We
155 co-stained *Slc17a7* (Vglut1), *Slc17a6* (Vglut2), or *Slc17a8* (Vglut3) with *Dbh* respectively in brain
156 tissue of adult mice and characterized the colocalization of *Slc17a7, Slc17a6, Slc17a8* with *Dbh* in
157 brainstem NA nuclei A7, LC, A5, sub CD/CV, anterior C1/A1 and C2/A2, posterior C1/A1 and
158 C2/A2, and C3 (Figure 2A-C and Figure 2 supplement 2A-B). No *Slc17a7/Dbh* double positive
159 neurons were detected in any part of the central NA system, consistent with our fate map.
160 *Slc17a8* mRNA colocalization with *Dbh* was only found in the posterior part of C2/A2 where 27.1
161 $\pm$ 1.86% of *Dbh* positive neurons demonstrated *Slc17a8* colocalization, again consistent with our
162 fate map. However, we only found detectable levels of *Slc17a6* mRNA in the C1/A1, C2/A2 and
163 C3 NA regions, but not in the A7, LC, A5, sub CD/CV. The percentages of *Slc17a6/Dbh* double
164 positive neurons for regions where detected were as follows: 84.7 $\pm$ 5.82% in anterior C1/A1,
165 66.3 $\pm$ 0.335% in anterior C2/A2, 35.7 $\pm$ 3.01% in posterior C1/A1, 90.1 $\pm$ 2.45% in posterior
166 C2/A2, and 79.7 $\pm$ 3.94% in C3. This result is consistent with the previous *in situ* data in adult rats
167 (Stornetta et al., 2002a, 2002b) suggesting that there is no obvious expression difference of
168 *Slc17a6* in the central NA system between mouse and rat. However, the *Slc17a6 in situ* data did
169 not show expression in anterior NA populations. This difference between our *in situ* data and fate
170 map data supports our previous hypothesis that many NA neurons expressed *Slc17a6* (Vglut2) at
171 some point from early development toward adulthood but the expression of *Slc17a6* (Vglut2) is
172 diminished during adulthood. Interestingly, Yang et al. (2021) did show adult Vglut2 co-
173 expression in LC by a viral injection of both Cre and Flpo-dependent eYFP into the LC of a bi-

174 transgenic mouse with both *Th*^{Flpo} and *Slc17a6*^{Cre}. To verify this result, we injected an AAV virus
175 containing Cre-dependent tdTomato (pAAV-EF1a-DIO-tdTomato-WPRE) into the LC region of
176 adult *Slc17a6*^{Cre} mice. Consistent with Yang et al. (2021), we observed sparse Vglut2-Cre and TH-
177 immunopositive double labelled neurons in the LC (Figure 2 supplement 1). Additionally, Souza
178 et al. (2022a) showed about 28.5% of A5 neurons are *Slc17a6* mRNA positive in adult rats by RNA
179 scope, a method which is more sensitive than the traditional *in situ* hybridization we used here.
180 These data suggest that some adult NA neurons in LC and A5 have *Slc17a6* (Vglut2) co-expression,
181 but the *Slc17a6* mRNA level cannot be detected by traditional *in situ* hybridization.
182
183 **Vglut2 expression is effectively knocked down in the whole central noradrenergic system in**
184 **Dbh-Cre; Vglut2 cKO mice**
185 To investigate the requirement of Vglut2-based glutamatergic signaling in the central NA system
186 in breathing under physiological challenges, we used Dbh-Cre; *Slc17a6*$^{flox/flox}$ (Dbh-Cre; Vglut2
187 cKO) to remove Vglut2 expression from all noradrenergic neurons. This is the same model used
188 by Abbott et al. (2014) to show that Vglut2 expression in the NA system was required for an
189 increase in respiratory frequency following unilateral optogenetic stimulation of anterior C1. To
190 verify if Vglut2 expression was effectively removed from central NA neurons in Dbh-Cre; Vglut2
191 cKO mice, we used fluorescent mRNA *in situ* hybridization for *Slc17a6* (Vglut2) and *Dbh* in the
192 mouse brainstems and compared the *Slc17a6* (Vglut2) signal intensity in *Dbh* positive neurons in
193 Dbh-Cre; Vglut2 cKO mice to their littermate controls. We found that *Slc17a6* mRNA expression
194 was 96.4 $\pm$ 0.226% decreased compared to controls, indicating that the *Slc17a6* (Vglut2) was
195 effectively recombined to abrogate expression in NA neurons (Figure 3A-B and Figure 3
196 supplement 1).
197
198 **Vglut2-based glutamatergic signaling in central NA neurons is not required for baseline**
199 **breathing nor for the hypercapnic ventilatory reflex under distinct CO_2 challenges**
200 Multiple prior studies provide indirect evidence that NA glutamate transmission may play roles
201 in respiratory function, particularly that anterior C1 neurons mediate the hypoxic ventilatory
202 response through the pFRG/RTN and/or the NA A5 group (Malheiros-Lima et al., 2022, 2020).

203 Additionally, the A5 group has been implicated in the hypercapnic reflex (Haxhiu et al., 1996).
204 Thus, we sought to determine if Vglut2-based glutamatergic signaling in central NA neurons is
205 necessary to regulate baseline breathing and the hypercapnic chemoreflex in unanesthetized and
206 unrestrained animals. We used whole-body barometric plethysmography to measure the
207 breathing and metabolism of unanesthetized and unrestrained mice. After a five-day habituation
208 protocol, the respiratory responses of Dbh-Cre; Vglut2 cKO mice and their littermate controls,
209 including the overall respiratory output or ventilatory equivalent of oxygen (V_E/V_{O2}), respiratory
210 rate (V_f), tidal volume (V_T), minute ventilation (V_E), metabolic demand (V_{O2}), inspiratory duration
211 (T_I), expiratory duration (T_E), breath cycle duration (T_{TOT}), inspiratory flow rate (V_T/T_I), and
212 expiratory flow rate (V_T/T_E), were measured under room air and hypercapnia (5% CO_2) (Figure
213 4A). 5% CO_2 gas challenge produced a significant change in all the respiratory parameters
214 compared to room air in both Dbh-Cre; Vglut2 cKO and control mice. However, surprisingly, Dbh-
215 Cre; Vglut2 cKO mice did not show significant differences in any respiratory or metabolic
216 parameter mentioned above compared to their littermate controls under both room air and 5%
217 CO_2 challenges (Figure 4B and Table 1-2). In addition, to investigate if Vglut2-based NA derived
218 glutamate is required for regulating the dynamic patterns of breathing, such as the breathing
219 rhythms, we generated Poincaré plots for T_I, T_E, T_{TOT}, V_T/T_I, V_T/T_E, V_f, V_T, and V_E and we calculated
220 the SD1 and SD2 statistics for each parameter under room air and 5% CO_2. We found that Dbh-
221 Cre; Vglut2 cKO mice only showed a marginally statistically significant increase in the SD1 of
222 inspiratory duration (T_I) ($p=0.0492$). Outside of this single comparison, however, we found no
223 significant differences in the other parameters between the two groups (Figure 4 supplement
224 4A-H). Thus, we theorize that the statistically significant result for the SD1 of T_I seen here is likely
225 either a result of measurement noise or a consequence of a type 1 error. The overall pattern of
226 results suggested that Vglut2-based glutamatergic signaling is not required for regulating either
227 the steady state of or the dynamic patterns of baseline breathing and hypercapnic ventilatory
228 reflex under 5% CO_2.
229
230 To further investigate the role of Vglut2-based glutamatergic signaling in the hypercapnic
231 response, we interrogated the system further with more severe hypercapnic exposures and

232 measured the breathing of Dbh-Cre; Vglut2 cKO mice under 7% CO_2 and 10% CO_2. Both 7% and
233 10% CO_2 stimuli produced a significant respiratory response in both mutant and control mice.
234 Under the 7% CO_2 condition, Dbh-Cre; Vglut2 cKO mice showed a significantly decreased tidal
235 volume (V_T) (p=0.023) and a significantly reduced inspiratory flow rate (V_T/T_I) (p=0.0016), but the
236 overall respiratory output (V_E/V_{O2}), respiratory rate (V_f), minute ventilation (V_E), metabolic
237 demand (V_{O2}), inspiratory duration (T_I), expiratory duration (T_E), breath cycle duration (T_{TOT}), and
238 expiratory flow rate (V_T/T_E) did not show a significant difference between the mutant mice and
239 their sibling controls (Figure 5A-B and Table 3). Additionally, none of the dynamic patterns of any
240 respiratory parameter showed a significant difference between the mutant and control groups
241 (Figure 5 supplement 1A-H). This result suggests that Vglut2-based glutamatergic signaling in
242 central NA neurons is not required for regulating the hypercapnic ventilatory reflex and breathing
243 regularity under 7% CO_2.
244
245 Under 10% CO_2 challenge, none of the steady state breathing parameters including the overall
246 respiratory outputs (V_E/V_{O2}), respiratory rate (V_f), tidal volume (V_T), minute ventilation (V_E),
247 metabolic demand (V_{O2}), inspiratory duration (T_I), expiratory duration (T_E), breath cycle duration
248 (T_{TOT}), inspiratory flow rate (V_T/T_I), and expiratory flow rate (V_T/T_E) were significantly different
249 between Dbh-Cre; Vglut2 cKO mice and their littermate controls, suggesting that Vglut2-based
250 glutamatergic signaling in central NA neurons is not required for the hypercapnic ventilatory
251 reflex under 10% CO_2 (Figure 6A-B and Table 4). For the dynamic patterns of breathing, the SD1
252 of breath cycle duration (T_{TOT}) (p=0.028) and SD1 of respiratory rate (V_f) (p=0.038) showed a
253 significant increase in mutant mice compared to the controls (Figure 6 supplement 1A-H). This
254 suggests that removing Vglut2 from central NA neurons may increase the breathing irregularity
255 under high CO_2 challenges like 10% CO_2.
256
257 **Vglut2-based glutamatergic signaling in central NA neurons is not required for the hypoxic**
258 **ventilatory reflex under 10% O_2**
259 To determine if Vglut2-based glutamatergic signaling in central NA neurons is necessary to
260 regulate the hypoxic chemoreflex, we measured the ventilation response of Dbh-Cre; Vglut2 cKO

261 mice under 10% O_2. We analyzed the ten respiratory parameters in three 5-min epochs following
262 10% O_2 challenge onset. Similar to the hypercapnic challenges, the 10% O_2 challenge produced a
263 significant breathing response in every 5-min epoch compared to room air, but no significant
264 difference was found in the overall respiratory output (V_E/V_{O2}), respiratory rate (V_f), tidal volume
265 (V_T), minute ventilation (V_E), metabolism demand (V_{O2}), inspiratory duration (T_I), expiratory
266 duration (T_E), breath cycle duration (T_{TOT}), inspiratory flow rate (V_T/T_I), and expiratory flow rate
267 (V_T/T_E) between Dbh-Cre; Vglut2 cKO mice and controls in any of the three 5-min 10% O_2 epochs
268 (Figure 7A-B and Table 5). These data suggest that Vglut2-based glutamatergic signaling in central
269 NA neurons is not required for the hypoxic ventilatory reflex under 10% O_2. For the dynamic
270 patterns of breathing, the SD2 of inspiratory flow rate (V_T/T_I) (p=0.005) and the SD2 of minute
271 ventilation (V_E) (p=0.026) were significantly increased during the first epoch (first 5 minutes)
272 under the 10% O_2 challenge in mutant mice, suggesting that Vglut2-based glutamate may play a
273 role in maintaining breathing regularity during the initial, or reflexive, response to hypoxia (Figure
274 7 supplement 1A-H).
275
276 **Discussion**
277 Neuron co-transmission of two or more neurotransmitters across excitatory, inhibitory, and
278 neuro-modulatory facets is becoming an increasingly appreciated phenomenon in the central
279 nervous system. Functional interrogation of co-transmission is essential not only to understand
280 the distinct and cooperative roles that multiple signaling molecules may play at the synapse but
281 also to determine the most critical targets for potential therapeutics. To our knowledge, the
282 unopposed paradigm in the field until now has been that vesicular glutamate transporter 2
283 (Vglut2)-based glutamate transmission from central noradrenergic neurons is important in
284 respiratory homeostasis. Anatomically, it has long been appreciated that central NA neurons co-
285 express Vglut2, the major glutamate marker among three glutamate transporters (DePuy et al.,
286 2013; Souza et al., 2022a; Stornetta et al., 2002a, 2002b; Yang et al., 2021). Also, it has been well
287 documented that NA Vglut2 positive fibers innervate known central respiratory centers or other
288 autonomic centers, that, when perturbed, could potentially disrupt respiratory homeostasis
289 (Supplemental Table 1). Functionally, multiple reports have suggested that Vglut2-based

290 glutamate transmission plays a role in respiratory homeostasis (Abbott et al., 2014;
291 Malheiros-Lima et al., 2022, 2020, 2018). It has also been suggested that, at least for C1 neurons,
292 the apparent lack of a plasmalemmal monoamine transporter may attenuate or eliminate
293 noradrenergic or adrenergic release from these fibers (Guyenet et al., 2013). However, as
294 discussed below, much of the functional evidence supporting a role for Vglut2-based glutamate
295 transmission from central noradrenergic neurons in breathing is circumstantial or of a non-
296 physiological nature, and absent or attenuated release of adrenaline and noradrenaline has not
297 been demonstrated. Nonetheless, the dominant perspective that NA-Vglut2 glutamate
298 transmission plays a role in breathing has remained unchallenged. Our studies, in contrast to
299 prior work, show that loss of Vglut2 in NA neurons does not appreciably change baseline or
300 chemosensory breathing in unanesthetized and unrestrained mice. Additionally, our work
301 uncovers a novel dynamic expression pattern for Vglut2 and an entirely undescribed co-
302 expression domain for Vglut3 in central NA neurons.
303
304 Vglut2 has been shown to be co-expressed in subsets of central NA neurons, however, to our
305 knowledge, the potential for the central NA neurons to express the other glutamate transporters
306 Vglut1 or Vglut3 has not been reported at the anatomical level. To determine if central NA
307 neurons express either Vglut1 or Vglut3 and to confirm the Vglut2 expression, we carried out
308 cumulative intersectional fate mapping using *Slc17a7*^{Cre}; *Dbh*$^{p2a\text{-}Flpo}$; *Rosa26*$^{RC::FLTG}$, *Slc17a6*^{Cre};
309 *Dbh*$^{p2a\text{-}Flpo}$; *Rosa26*$^{RC::FLTG}$ and *Slc17a8*^{Cre}; *Dbh*$^{p2a\text{-}Flpo}$; *Rosa26*$^{RC::FLTG}$ compound mouse lines. As this
310 approach maps the cumulative history of expression, we also examined acute adult expression
311 of *Slc17a7* (Vglut1), *Slc17a6* (Vglut2) and *Slc17a8* (Vglut3) using fluorescent RNA *in situ*
312 hybridization. Our *in situ* results for *Slc17a6* (Vglut2) agreed with earlier published outcomes
313 (DePuy et al., 2013; Stornetta et al., 2002a, 2002b) showing as much as 80% expression in
314 posterior NA neurons. However, there was no appreciable signal in anterior groups (A7, LC, A5,
315 sub CD/CV). This lack of expression was in stark contrast to the cumulative fate map for Vglut2,
316 showing as much as 75% of the anterior central NA neurons were recombined by the Vglut2-Cre
317 over the lifetime of the animal. To further interrogate the acute activity of the Vglut2-Cre in the
318 Locus Coeruleus in the adult mouse, we injected a Cre responsive virus in LC of *Slc17a6*^{Cre} mice

319 and found sparse Vglut2-Cre positive NA neurons in the LC. The outcomes from the cumulative
320 fate map and acute injections are in agreement with published results from Yang et al. (2021).
321 Notably, our use of the *Dbh*$^{p2a\text{-}Flpo}$ avoided expression in the parabrachial nucleus (PBN), which
322 was a confounding variable in the *Th*^{Flpo} mouse. In addition, 28.5% of A5 neurons were shown to
323 be *Slc17a6* (Vglut2) positive in adult rats by RNA scope (Souza et al., 2022b). It is notable that
324 both our lab and the work published by (Stornetta et al., 2002a, 2002b) failed to detect *Slc17a6*
325 (Vglut2) expression in anterior groups, but that apparently very low levels can be detected by
326 more sensitive recombinase and RNA scope methods. Additional electrophysiological evidence
327 suggests that this expression is functional (Yang et al., 2021). However, it is notable that we see
328 nearly 80% of the LC and 85% of A5 recombined in the intersectional strategy representing
329 lifetime expression, but our study and others find only 20% of the LC and 28.5% of A5 may be
330 expressing *Slc17a6* (Vglut2) at any given moment in adults. Thus, it suggests that Vglut2 co-
331 expression in anterior NA groups is time dependent, though the underlying temporal dynamics
332 of Vglut2 remain unknown. We hypothesize that this could be either a temporal restriction in
333 expression as the animal matures or may reflect dynamic change driven by behavioral or
334 physiological experiences, which could be tested with the use of inducible conditional strategies.
335
336 For *Slc17a7* (Vglut1), neither fate map nor *in situ* hybridization revealed any co-expression within
337 the central NA system. However, *Slc17a8* (Vglut3) expression was found in the posterior part of
338 NA neurons including C2/A2 and C1/A1. This study is the first to characterize this expression. The
339 majority of this Vglut3 co-expression is restricted to the posterior part of the C2/A2 NA
340 population. This NA region has not been heavily implicated in respiratory control nonetheless it
341 readily lends itself to interrogation by intersectional genetic methods and *in situ* hybridization.
342 Given its distal expression from anterior C1, it is less likely that Vglut3 would compensate for loss
343 of Vglut2 in anterior C1, though this has not been ruled out. Further, while Vglut3 is a marker of
344 glutamatergic neurons, its role in neurotransmission is not wholly defined as Vglut3 is typically
345 found in soma and dendrites (Fremeau et al., 2004).
346

347 The cumulative fate map and *in situ* hybridization experiments were performed in both females
348 and males and no obvious sex difference was observed in the expression pattern of Vglut1, Vglut2
349 or Vglut3. However, only three mice were characterized in each dataset, thus, larger sample sizes
350 may capture more subtle outcomes for potential sex differences.
351
352 Based on the Vglut2 co-expression in NA neurons and their projections to multiple brain regions
353 important in respiration, several studies suggest that glutamate in NA populations is important
354 in breathing control. However, the evidence those studies provided is circumstantial, indirect, or
355 limited due to experimental caveats or technical limitations. Abbott et al. (2014), using exactly
356 the same mouse model as this study, showed that conditionally knocking out Vglut2 in the whole
357 central NA system did not significantly change respiratory rate under room air, which is
358 consistent with our findings here. Our results differ in that they reported removing Vglut2 from
359 central NA neurons attenuated an increase in respiratory rate resulting from unilateral C1
360 optogenetic stimulation. However, while the optogenetic stimulation of C1 neurons did drive a
361 Vglut2 dependent increase in respiratory rate, it is not clear if the resulting change in breathing
362 reflects a native feature of the network that might be engaged in chemosensory responses or
363 other aspects of breathing. It remains possible that strong unilateral optogenetic stimulation (up
364 to 20Hz) of a small, isolated population drives a Vglut2 dependent, but ectopic, function that is
365 not typically engaged in the normal operation of the breathing network. Such ectopic outcomes
366 could come from several potential, non-exclusive mechanisms. First, unilateral stimulation could
367 drive a network hysteresis or dysregulation similar to a focal injury that is not a typical biological
368 feature (Ducros et al., 2003). This point is well made in Abbott et al. (2013) in their discussion of
369 C1 optogenetic stimulation where they state, "resulting cardiorespiratory response pattern
370 should not be considered strictly "physiological," because a physiological response is never
371 initiated by selective activation of a single cluster of CNS neurons and the various subsets of C1
372 neurons are presumably never recruited en bloc under any physiological condition". Second,
373 strong stimulation could result in overwhelming synaptic mechanisms (i.e., glial uptake) resulting
374 in glutamate spillover and unintended cross talk to affect extra-synaptic neurons proximal to
375 targeted NA fibers. Activity dependent spillover transmission has been documented elsewhere

376 in the nervous system (Henneberger et al., 2020; Hülsmann et al., 2000). Third, the outcomes
377 could be secondary to a different autonomic or behavioral function requiring NA-derived
378 glutamatergic signaling involving metabolism or circulation (DePuy et al., 2013; Yang et al.,
379 2021). Additionally, respiratory parameters except for respiratory rate (V_f), such as tidal volume
380 (V_T) and minute ventilation (V_E) were not reported, making comprehensive comparison difficult.
381
382 More circumstantially, Malheiros-Lima et al. (2020) suggested C1 neurons potentially release
383 glutamate at the pFRG site to regulate active expiration under hypoxia in anesthetized rats by
384 providing three indirect lines of evidence: 1) Vglut2-expressing C1 neurons project to the pFRG
385 region; 2) Increased abdominal expiratory nerve activity (Abd_{EMG}) was blunted after blockade of
386 ionotropic glutamatergic receptors at the pFRG site under anesthesia using cytotoxic KCN
387 mediated hypoxia; and 3) Depletion of C1 neurons eliminated the increased Abd_{EMG} elicited by
388 hypoxia. However, 1) the glutamatergic signaling targeting the pFRG region is not necessarily
389 from C1 NA neurons since glutamatergic neurons from other regions also project to the pFRG site
390 (Yang and Feldman, 2018). Thus, it is possible that the glutamatergic signaling that is required for
391 hypoxic response is derived from other glutamatergic neurons such as the preBötzinger complex
392 and the RTN itself. Furthermore, 2) C1 neuron depletion knocks out all the signaling modalities
393 in the C1 population including both noradrenaline and glutamate. It is not clear which signaling
394 drives the hypoxic response. Finally, 3) KCN injection mimics a hypoxic challenge by activating
395 peripheral chemoreceptors, but the physiological responses differ from those seen during
396 environmental hypoxia exposure. Thus, the abdominal activity changes due to KCN injection may
397 not be recaptured under physiological hypoxic challenge.
398
399 Similarly, Malheiros-Lima et al. (2022) and Malheiros-Lima et al. (2018) showed that Vglut2-
400 expressing C1 neurons project to both the NA A5 region and the preBötzinger complex. The
401 blockade of ionotropic glutamatergic receptors at the A5 region or preBötzinger complex reduced
402 the increase in phrenic nerve activity and the breathing frequency caused by optogenetic
403 stimulation of C1 cells in an anesthetized preparation. Together these results suggest that Vglut2-
404 expressing C1 neurons communicate with A5 or preBötzinger complex neurons by releasing

405 glutamate in turn to regulate phrenic nerve activity or breathing frequency. Again, these two
406 studies showed that C1 neurons are important to regulate phrenic nerve activity or breathing
407 frequency, however, it is not necessarily through a direct C1-A5 or C1-preBötzinger complex
408 glutamatergic pathway, whereas an indirect multi-synaptic pathway originating with C1
409 noradrenaline and ending with glutamate transmission from an intermediate to A5 or
410 preBötzinger complex cannot be ruled out. Importantly, in all four studies noted here, respiratory
411 measurements were limited or proxies of breathing under anesthesia were used. The role of NA-
412 Vglut2 signaling was not reported in the context of an unanesthetized, unrestrained animal under
413 normoxic, hypoxic, or hypercapnic breathing in these previous studies.
414
415 Thus, the limitations and indirect lines of the evidence in these studies raised the question as to
416 whether or not glutamatergic signaling in central NA neurons is required or necessary to
417 modulate respiratory homeostasis under more physiologically relevant circumstances and if NA-
418 derived glutamate is an important mechanism to understand the pathophysiology of NA neurons
419 in respiratory diseases. The goal of our study was to test the requirement of NA-based
420 glutamatergic signaling in breathing homeostasis in the unanesthetized and unrestrained animal
421 under conditions that would engage the whole respiratory control network rather than a singular
422 component that may drive hysteresis or artifactual outcomes. Our *in vivo* breathing data under
423 room air, hypoxic, and multiple hypercapnic conditions failed to show the requirement of NA-
424 derived Vglut2 in normal breathing and respiratory chemoreflexes directly. For the dynamic
425 patterns of breathing, we measured the SD1 and SD2 of eight parameters under each gas
426 condition. We found no consistent change across multiple hypercapnic challenges or hypoxia.
427 We did find that under severe hypercapnic challenge (10% CO_2), NA derived Vglut2 removal
428 resulted in an increase in the SD1 of breath cycle duration and respiratory rate, which was not
429 observed under 5% and 7% CO_2 conditions. Under hypoxia (10% O_2), Dbh-Cre; Vglut2 cKO mice
430 only showed an increase in the SD2 of inspiratory flow rate and minute ventilation during the
431 first 5-minute of 10% O_2 exposure. These findings may suggest that Vglut2-based glutamatergic
432 signaling in central NA neurons may play a role in modulating breathing regularity under high CO_2

433 challenge and hypoxia. However, the phenotypes were of a small magnitude and not consistent
434 across challenges, and not at all seen under homeostatic breathing.
435
436 To ensure a rigorous and robust conclusion, we included several extra precautions and additional
437 measures in our experimental design and analysis. First, we use exactly the same mouse model,
438 DBH-Cre; Vglut2 cKO, as Abbott et al. (2014) used, and confirmed, by a second method
439 (fluorescent RNA *in situ* hybridization) that Vglut2 expression was indeed abrogated in the whole
440 central NA system. Our results are in strong agreement with DePuy et al. (2013) that
441 recombination is efficient. Notably, we assayed for expression at the cell body, rather than the
442 fibers and see no singular cell body that is scored positive. Second, we measured the breathing
443 of unanesthetized, unrestrained, and habituated mice under physiological challenges including
444 normoxia, hypercapnia and hypoxia. Third, to visualize breathing function comprehensively, the
445 metabolic parameter and multiple respiratory parameters (both the steady state and the
446 dynamic patterns) were measured and reported in absolute values including oxygen
447 consumption, respiratory rate, tidal volume, minute ventilation, overall respiratory output
448 (minute ventilation normalized to oxygen consumption), inspiratory duration, expiratory
449 duration, breath cycle duration, inspiratory flow rate, and expiratory flow rate. Fourth, our
450 experimental design was overpowered (i.e., n=16-21 vs 5-13 needed for power based on power
451 analysis and n=7-8 reported in other manuscripts). Each respiratory/metabolic parameter for
452 each physiological condition including room air, hypercapnia, and hypoxia was derived by
453 quantifying the entire respiratory trace and analyzed between mutant and sibling controls by
454 using a linear mixed-effects regression model with animal type (experimental vs. control) as fixed
455 effects, animal ID as a random effect, and sex as an experimental covariate (for which we did not
456 find a significant effect) (Lusk et al., 2023).
457
458 Despite our experimental design and the extensive nature of our measurements, there remain
459 several possibilities or considerations in the interpretation of our data. The first possibility is
460 Vglut3 in posterior CA domain (first characterized in this study) compensates for the effect of the
461 loss of Vglut2 in NA neurons in breathing. However, we argue that this is unlikely because 1) Our

462 model is the same used in the other study where a Vglut2-dependent effect was seen with
463 optogenetic stimulation. 2) Vglut3 is expressed in the posterior C2/A2 NA neurons which are
464 anatomically distant from anterior C1 and the LC (the two most likely NA candidates with Vglut2
465 co-expression to impact breathing). Also, posterior C2/A2 hasn't been heavily implicated in
466 breathing regulation. Future work will need to further investigate the role of Vglut3 in posterior
467 CA in respiratory control in order to test this possibility. The second possibility is that pre- or post-
468 natal developmental compensation corrects for the loss of NA derived glutamate. Again, we
469 argue that is unlikely, as 1) we are using the same adult model that provided the most direct
470 evidence and first functionally demonstrated a potential role for C1-derived glutamate in
471 breathing; 2) Abbott et al. (2014) highlight that C1 NA neurons showed no obvious abnormalities
472 in number, morphology, and projection patterns after knocking out Vglut2; and 3) we have
473 examined the requirement of NA-expressed Vglut2 in P7 neonate mice in the autoresuscitation
474 reflex and saw no differences (data not shown). However, it is still possible that developmental
475 compensation occurs before P7, which is something that could be better tested by using the Dbh-
476 CreERT2 (Stubbusch et al., 2011) to more acutely remove Vglut2 expression (though this leaves
477 a window of 2-3 weeks for compensation to occur). Third, as we only address the loss of NA-
478 Vglut2 based signaling across the entire NA system, it remains a formal possibility that this
479 ultimately results in the removal of Vglut2 dependent signaling from two counter balancing
480 regions of the NA system and are therefore left with null results whereas removal from anterior
481 C1 alone would show a requirement. To test this possibility, it would require an intersectional
482 conditional knockout/loss of function approach, something that has not yet been shown to be
483 efficient and effective and would be beyond the scope of these studies. Fourth, it is possible that
484 another neurotransmitter/neuropeptide within NA neurons might be released in higher amounts
485 in Dbh-Cre; Vglut2 cKO mice to compensate for the deficiency of glutamate in breathing.
486 Neuropeptide Y (NPY) and galanin have been shown to co-exist in LC NA neurons and are involved
487 in regulating energy metabolism, stress, or anxiety (Ruohonen et al., 2012; Tasan et al., 2010;
488 Weinshenker and Holmes, 2016). In our studies, we account for potential metabolic changes that
489 may underlie or be coordinate with changes in breathing. However, we did not test for potential
490 changes in blood pressure or other autonomic functions as well as affective state that may, in

491 some obscure way, compensate for changes in breathing. Further interrogation of NPY or galanin
492 signaling across NA neurons and potential compensatory effects in breathing through changes in
493 metabolism or other autonomic function under stress or anxiety may yield notable insights.
494 Lastly, our results are loss of function in nature. We do not test sufficiency or gain of function and
495 cannot fully rule out a role for NA-Vglut2 based glutamatergic signaling in the control of
496 breathing.
497
498 From a translational perspective, our data question whether or not glutamatergic signaling in NA
499 neurons is likely to be a key mechanism and therefore a therapeutic target for breathing
500 disorders, such as Rett syndrome and SIDS. *Mecp2*-deficient mice (a mouse model of Rett
501 Syndrome that phenocopies many human symptoms) showed both a deficiency of NA
502 populations (reduced number of NA neurons in C2/A2 and C1/A1 group) and highly variable
503 respiratory rhythm at around 4-5 weeks of age (Roux et al., 2007; Viemari et al., 2005). 80% of
504 Rett Syndrome patients experience breathing issues, such as unstable breathing, episodes of
505 hyperventilation, and breath holds, throughout their lifespan (Ramirez et al., 2020). SIDS
506 decedents show NA abnormalities and are hypothesized to ultimately succumb from a failure in
507 cardiorespiratory autoresuscitation (Chigr et al., 1989; Garcia et al., 2013; Kopp et al., 1993;
508 Mansouri et al., 2001; Ozawa et al., 2003; Takashima and Becker, 1991). However, Dbh-Cre;
509 Vglut2 cKO mice, have normal baseline and chemosensory respiratory parameters as adults and
510 neonate mice show normal autoresuscitation indicating that perturbed NA based glutamatergic
511 signaling may not be a key driver in these or other related respiratory pathophysiologies.
512
513 In conclusion, our studies show that Vglut2 has a dynamic and extensive expression profile across
514 the central NA system. We were able to characterize a novel Vglut3-expressing NA population in
515 the posterior C2/A2 nuclei. Despite prior studies providing indirect and circumstantial evidence
516 that noradrenergic-based glutamatergic signaling may play a role in control of breathing, our
517 conditional loss of function studies in adult unanesthetized and unrestrained mice failed to
518 consistently and significantly change room air breathing, the hypercapnic ventilatory reflex, and
519 the hypoxic ventilatory reflex. These outcomes offer a contrasting perspective from the current

field view and provides further insight into the potential role of NA-glutamate transmission in the control of breathing and NA neuron dysfunction in respiratory disorders.

Materials and Methods

Ethical Approval

Studies were approved by the Baylor College of Medicine Institutional Animal Care and Use Committee (IACUC) under protocol AN-6171, and all experiments reported here were performed in accordance with relevant guidelines and regulations.

Breeding, Genetic Background, and Maintenance of Mice

We maintained all our heterozygous mouse strains by backcrossing to wildtype C57BL/6J mice and homozygous mouse strains by sibling crosses. For immunofluorescence experiments, heterozygous B6;129S-*Slc17a7*$^{tm1.1(cre)Hze}$/J (*Slc17a7*^{Cre}, Vglut1-Cre) (Jax Stock No: 023527), *Slc17a6*$^{tm2(cre)Lowl}$/J (*Slc17a6*^{Cre}, Vglut2-Cre) (Jax Stock No: 016963) *and* B6;129S-*Slc17a8*$^{tm1.1(cre)Hze}$/J (*Slc17a8*^{Cre}, Vglut3-Cre) (Jax Stock No: 018147) were mated with heterozygous *Dbh*$^{em2.1(flpo)Rray}$ (*Dbh*$^{p2a\text{-}Flpo}$, DBH-p2a-Flpo) (MMRRC ID: 41575) (Sun and Ray, 2016) mice respectively to derive compound lines with both Cre and Flpo alleles (*Slc17a7*^{Cre}; *Dbh*$^{p2a\text{-}Flpo}$, *Slc17a6*^{Cre}; *Dbh*$^{p2a\text{-}Flpo}$, and *Slc17a8*^{Cre}; *Dbh*$^{p2a\text{-}Flpo}$). Then these three compound lines were each mated with homozygous B6.Cg-*Gt(ROSA)26Sor*$^{tm1.3(CAG\text{-}tdTomato,\text{-}EGFP)Pjen}$/J (*Rosa26*$^{RC::FLTG}$) (Jax Stock No: 026932) to derive three different intersectional mouse lines *Slc17a7*^{Cre}; *Dbh*$^{p2a\text{-}Flpo}$; *Rosa26*$^{RC::FLTG}$, *Slc17a6*^{Cre}; *Dbh*$^{p2a\text{-}Flpo}$; *Rosa26*$^{RC::FLTG}$ and *Slc17a8*^{Cre}; *Dbh*$^{p2a\text{-}Flpo}$; *Rosa26*$^{RC::FLTG}$. For *in situ* hybridization experiments, wildtype C57BL/6J mice were ordered from the Center of Comparative Medicine (CCM), Baylor College of Medicine. For NA-Vglut2 conditional loss of function *in situ* hybridization and plethysmography experiments, hemizygous transgene Tg(Dbh-cre)KH212Gsat (Dbh-Cre) (MMRRC ID: 036778-UCD GENSAT) mice were mated with homozygous *Slc17a6*^{tm1Lowl}/J *(Slc17a6*$^{flox/flox}$*)* (Jax Stock No: 012898) to derive Dbh-Cre; *Slc17a6*$^{flox/+}$. Dbh-Cre; *Slc17a6*$^{flox/+}$ mice were mated with *Slc17a6*$^{flox/flox}$ to derive Dbh-Cre; *Slc17a6*$^{flox/flox}$ (Dbh-Cre; Vglut2 cKO). Sibling mice that lacked the Cre allele or carried the Cre allele but lacked the floxed Vglut2 alleles were used as controls. Rosa26 specific primers for the *Rosa26*$^{RC::FLTG}$ mice were 5'-

549 GCACTTGCTCTCCCAAAGTC, 5'-GGGCGTACTTGGCATATGAT, and 5'-CTTTAAGCCTGCCCAGAAGA
550 (Ray et al., 2011) and yield a 495 bp band (targeted) and 330 bp band (wt). Cre-specific primers
551 for all Cre drivers were 5'-ATCGCCATCTTCCAGCAGGCGCACCATTGCCC and 5'-
552 GCATTTCTGGGGATTGCTTA and yielded a 550 bp band if positive. Flpo-specific primers for *Dbh*$^{p2a-}$
553 ^{Flpo} are 5'- CACGCCCAGGTACTTGTTCT and 5'-CCACAGCAAGAAGATGCTGA (Sun and Ray, 2016)
554 and yielded a 226 bp band if positive. *Slc17a6*^{flox} specific primers for Vglut2-floxed mice are
555 available at The Jackson Laboratory website (https://www.jax.org/strain/012898).
556
557 **Immunofluorescence staining**
558 *Slc17a7*^{Cre}; *Dbh*$^{p2a-Flpo}$; *Rosa26*$^{RC::FLTG}$, *Slc17a6*^{Cre}; *Dbh*$^{p2a-Flpo}$; *Rosa26*$^{RC::FLTG}$ and *Slc17a8*^{Cre}; *Dbh*$^{p2a-}$
559 ^{Flpo}; *Rosa26*$^{RC::FLTG}$ adult mice of both sexes were sacrificed and transcardially perfused with 0.1
560 M phosphate-buffered saline (PBS) then with 4% paraformaldehyde (PFA) in PBS. Mouse brains
561 were dissected out and fixed for 2h in 4% PFA before a PBS rinse and dehydration in 30% sucrose
562 in PBS. Brains were embedded in OCT blocks, sectioned at the thickness of 30µm, mounted on
563 slides, and stored at -80°C until they were ready for staining. The slides were hydrated in 0.1%
564 Triton-X in PBS (PBST) for 15 mins, blocked with 5% donkey serum in 0.1% PBST for 1h at room
565 temperature and then incubated with primary antibodies for 72 hours at 4°C in 0.1% PBST with
566 5% donkey serum. Tissues were washed in 0.1% PBST 3 times for 10 min each and then incubated
567 with secondary antibodies for 2hs at room temperature in 0.1% PBST with 5% donkey serum.
568 Slides were washed with 0.1% PBST for 10 min and washed in PBS twice for 10 min each, stained
569 for DAPI, washed 3 times for 10 min each with PBS and mounted in ProLong Glass (Invitrogen).
570 The following primary and secondary antibodies were used: chicken anti-GFP (1:1,000, Abcam
571 ab13970), rabbit anti-dsRed (1:1,000, Clontech 632496), donkey anti-chicken Cy2 (1:500, Jackson
572 703-225-155), donkey anti-rabbit Cy3 (1:500, Jackson 711-165-152).
573
574 **In situ hybridization**
575 Mouse brains were dissected out from adult mice of both sexes with 6-8 week of age, sectioned
576 into 25µm brain sections and mounted on slides. We generated a digoxigenin (DIG)-labeled
577 mRNA antisense probe against *Slc17a7* (Vglut1), *Slc17a6* (Vglut2), and *Slc17a8* (Vglut3) and

578 fluorescein (FITC)-labeled mRNA against *Dbh* using reverse-transcribed mouse cDNA as a
579 template and an RNA DIG or FITC-labeling kits from Roche (Sigma). Primer and probe
580 sequences for the *Slc17a7* (Vglut1), *Slc17a6* (Vglut2), and *Slc17a8* (Vglut3) and *Dbh* probes are
581 available in the Allen Brain Atlas (http://www.brain-map.org). For the *Slc17a6* (Vglut2) and *Dbh*
582 double ISH in Dbh-Cre; Vglut2 cKO and their littermate controls, we generated a new *Slc17a6*
583 (Vglut2) probe targeting exon 2 of *Slc17a6* specifically (Tong et al., 2007) and the probe sequence
584 is 892-1144bp as Slc17a6 transcript variant 1 and the size is 253bp. ISH was performed by the
585 RNA In Situ Hybridization Core at Baylor College of Medicine using an automated robotic
586 platform as previously described (Yaylaoglu et al., 2005) with modifications of the protocol for
587 double ISH. Modifications in brief [see Yaylaoglu et al. (2005) for buffer descriptions]: both
588 probes were hybridized to the tissue simultaneously. After the described washes and blocking
589 steps the DIG-labeled probes were visualized using tyramide-Cy3 Plus (1/75 dilution, 15-minute
590 incubation, Akoya Biosciences). After washes in TNT, the remaining HRP-activity was quenched
591 by a 10-minute incubation in 0.2M HCl. The sections were then washed in TNT, blocked in TNB
592 for 15 minutes, and incubated at room temperature for 30 minutes with HRP-labeled sheep anti-
593 FITC antibody (1/500 in TNB, Roche/Sigma). Following washes in TNT, the FITC-labeled probe was
594 visualized using tyramide-FITC Plus (1/50 dilution, 15-minute incubation, Akoya Biosciences).
595 Following washes in TNT, the slides were stained with DAPI (invitrogen), washed again, removed
596 from the machine, and mounted in ProLong Diamond (Invitrogen).
597
598 **Viral Injection**
599 To verify Vglut2 co-expression in LC in adult mice (Yang et al., 2021), 6-week-old *Slc17a7*^{Cre} mice
600 were injected with pAAV-EF1a-DIO-tdTomato-WPRE virus (RRID:Addgene_133786, obtained
601 from Joshua Ortiz at the Optogenetics and Viral Vectors Core at the Jan and Dan Duncan
602 Neurological Research Institute, 1ul at 7.90E+10 Gc/mL) into the LC (coordinates from bregma
603 anteroposterior −5.4 mm, lateral + 0.8 mm and dorsoventral – 4.0 mm) and allowed to incubate
604 for 4 weeks.
605
606 **Plethysmography**

607 Plethysmography on unanesthetized and free-moving mice was carried out as described in (Ray
608 et al., 2011). 6–8-week-old adult mice of both sexes with minimum group sizes n=16 were used
609 in both the experimental and control group for each experiment. Animals were subjected to a
610 five-day habituation protocol with each day including several minutes of handling, temperature
611 taken by rectal probe and at least 30 min exposure in the plethysmography chamber (Martinez
612 et al., 2019). Plethysmography started to be performed on the sixth day and was finished for all
613 animals within a week of the last day of habituation (Maximum 6 mice can be assayed for
614 plethysmography per day due to the limited number of plethysmography rigs). On the day of
615 testing, mice were taken out from their home cage, weighed, and rectal temperature was taken.
616 Animals were then placed into a flow-through, temperature-controlled (about 32°C with real-
617 time temperature recording) plethysmography chamber and allowed to acclimate for 20-40 mins
618 in room air (21% O_2/79% N_2) conditions. After acclimation (indicated by a steady respiratory trace
619 free from movement artifact), a 20-min baseline breathing trace was taken under room air, then
620 the chamber gas was switched to a hypercapnic or hypoxic mixture of 5% CO_2/21% O_2/74% N_2,
621 7% CO_2/21% O_2/72% N_2, 10% CO_2/21% O_2/69% N_2, or 10% O_2/90% N_2, depending on the protocol,
622 for 20 min. Chamber gas was then switched back to room air for another 20 min. The animals
623 were removed from the chamber and rectal temperature was measured immediately after the
624 mice were taken out from the chamber. Each testing period for an individual mouse was
625 separated by 24hs to allow for a full recovery.
626
627 **Plethysmography data analysis and statistics**
628 Details were previously described in (Martinez et al., 2019; Ray et al., 2011). Plethysmography
629 pressure changes were measured using a Validyne DP45 differential pressure transducer, CD15
630 carrier demodulator and a reference chamber, and were recorded with LabChart Pro in real time.
631 Respiratory waveforms were analyzed by the SASSI module of the Breathe Easy software to
632 determine respiratory frequency (V_f), tidal volume (V_T), minute ventilation (V_E), oxygen
633 consumption (V_{O2}), ventilatory equivalents for oxygen (V_E/V_{O2}), inspiratory duration (T_I),
634 expiratory duration (T_E), breath cycle duration (T_{TOT}), inspiratory flow rate (V_T/T_I), and expiratory
635 flow rate (V_T/T_E) (Lusk et al., 2023). Poincaré plots for T_I, T_E, T_{TOT}, V_T/T_I, V_T/T_E, V_f, V_T, V_E and their

636 SD1 and SD2 properties were generated and characterized by the STAGG module of the Breathe
637 Easy software. Analysis windows of the respiratory parameters were as follows: for room air, the
638 entire experimental period was considered; for hypercapnia, only the last 5 min challenge for
639 each of 5/7/10% CO_2 conditions were analyzed; and for hypoxia, three separate 5-min time
640 periods, namely the 5th-10th min, 10th-15th min, and 15th-20th min intervals, were used due to the
641 stereotypical biphasic respiratory response under this condition. Only steady quiescent breathing
642 periods were included in the data analysis. A power analysis was performed using the reported
643 effect size in Abbott et al. (2014), which used the same mouse model as we used here; 5-13 mice
644 were necessary to observe a statistically significant result (Abbott et al. (2014) was able to see a
645 significant difference between two groups with n=7 mice). In our experiments, the sample size
646 for each group (Dbh-Cre; Vglut2 cKO and control) exceeded 13. Steady state results (V_f, V_E, V_T,
647 V_{O2}, V_E/V_{O2}, T_I, T_E, T_{TOT}, V_T/T_I, V_T/T_E) for room air and hypercapnic or hypoxic data were compared
648 between Dbh-Cre; Vglut2 cKO cohorts and sibling controls using a linear mixed-effects regression
649 model with animal type (experimental vs. control) as fixed effects and animal ID as a random
650 effect (Lusk et al., 2023). SD1 and SD2 results for room air and hypercapnic or hypoxic data were
651 compared between Dbh-Cre; Vglut2 cKO cohorts and sibling controls using a Mann-Whitney U
652 test (Ferreira et al., 2022). A p-value threshold of $p < 0.05$ was used to test for statistical
653 significance. Individual data points, means, and standard errors of the mean are shown on all
654 charts. The graphs were plotted by Prism 8.
655
656 **Image quantification**
657 Images were taken by using a Zeiss upright epifluorescent microscope and a Zeiss LSM 880 with
658 Airyscan FAST confocal microscope. Images were captured using Zen software with z-stack
659 function from top to bottom with 0.34µm intervals, exported, and then analyzed in Imaris using
660 the spots and surface functions. For quantification of immunofluorescence staining, each GFP
661 positive area coincident with DAPI (to denote nuclear localization) was defined as Vglut2 or
662 Vglut3 expressing NA neurons while each tdTomato positive area coincident with DAPI was
663 defined as NA neurons without any Vglut2 or Vglut3 co-expression. For quantification of *Slc17a6*
664 (Vglut2) or *Slc17a8* (Vglut3) with *Dbh* double *in situ* hybridization in adult WT mice, *Dbh* positive

665 areas coinciding with DAPI were identified as NA neurons and the *Dbh* positive areas overlapped
666 with *Slc17a6* (Vglut2) or *Slc17a8* (Vglut3) positive pixels and DAPI were defined as NA neurons
667 colocalized with *Slc17a6* (Vglut2) or *Slc17a8* (Vglut3). The number of *Slc17a6* (Vglut2) or *Slc17a8*
668 (Vglut3) positive NA neurons and *Slc17a6* (Vglut2) or *Slc17a8* (Vglut3) negative NA neurons was
669 counted in each image for both immunofluorescence and *in situ* experiments and the percentage
670 of *Slc17a6* (Vglut2) or *Slc17a8* (Vglut3) positive NA neurons among all NA neurons in each NA
671 nucleus in each mouse brainstem was calculated every other brain section unilaterally. For
672 quantification of *Slc17a6* (Vglut2) and *Dbh* double ISH in Dbh-Cre; Vglut2 cKO and their littermate
673 controls, *Slc17a6* (Vglut2) pixel intensities in *Dbh* positive areas coincident with DAPI (NA
674 neurons) were measured in mutant and control images separately. The *Slc17a6* (Vglut2) pixel
675 intensity in NA neurons of control brains was normalized as 1 and the relative *Slc17a6* (Vglut2)
676 pixel intensity of NA neurons in mutant brains compared to that in control brains was calculated.
677 At least three mouse brains were examined for each set of experiments in each group. All
678 quantitative results were graphed using Prism 8.
679
680 **Data availability**
681 All the data supporting this study is available from the corresponding author upon request.
682
683 **Acknowledgments**
684 We thank the Optical Imaging & Vital Microscopy Core (OiVM) at Baylor College of Medicine with
685 the expert assistance of Jason Kirk for confocal imaging. We thank BCM Neuropathology Core
686 and Tao Lin for tissue sectioning. We thank the RNA In Situ Hybridization Core at Baylor College
687 of Medicine with the expert assistance of Cecilia Ljungberg for performing in situ hybridization
688 (NIH S10 OD016167 and NIH IDDRC Grant P50 HD103555). We thank Dr. Joshua Ortiz and Dr.
689 Benjamin Arenkiel at the NRI Optogenetics and Viral Vectors Core for providing Cre-responsive
690 AAV virus used in viral injection.
691
692 **Author contributions**

693 YC designed and completed immunofluorescence staining, imaging, and plethysmography
694 experiments, analyzed data, wrote the initial manuscript, and revised the manuscript.
695 SL completed the viral injection experiments and revised the manuscript.
696 AC updated the Poincaré function of Breathe Easy software, helped analyze the data, and revised
697 the manuscript.
698 CSW updated SASSI within Breathe Easy software, helped analyze the data, and revised the
699 manuscript.
700 RSR conceptualized and designed the study, analyzed the data, and helped write and revised the
701 manuscript.
702
703 **Competing interests**
704 No competing interests are declared.
705
706 **Figure 1. Cumulative fate maps of glutamate co-expressing NA neurons characterized by**
707 **intersectional genetics.** (A) Breeding schematic to generate the three intersectional reporter
708 lines *Slc17a7*^{Cre}; *Dbh*$^{p2a\text{-}Flpo}$; *Rosa26*$^{RC::FLTG}$, *Slc17a6*^{Cre}; *Dbh*$^{p2a\text{-}Flpo}$; *Rosa26*$^{RC::FLTG}$, *Slc17a8*^{Cre}; *Dbh*$^{p2a-}$
709 ^{Flpo}; *Rosa26*$^{RC::FLTG}$. In each of the three intersectional reporter crosses, NA neurons co-expressing
710 either Vglut1, Vglut2, or Vglut3 are labeled by green fluorescent protein (eGFP) while NA neurons
711 without any Vglut1,2, or 3 expressions are labelled by red fluorescent protein (tdTomato). Shown
712 as an example is the *Slc17a6*^{Cre}; *Dbh*$^{p2a\text{-}Flpo}$; *Rosa26*$^{RC::FLTG}$ (Vglut2-Cre/+; DBH-p2a-Flpo/+;
713 RC::FLTG/+) intersectional reporter line. (B) Quantification of the percentage of Vglut2-
714 coexpressing NA neurons among NA neurons in each brainstem NA nuclei including A7, LC, A5,
715 sub CD/CV, anterior C1/A1 and C2/A2, posterior C1/A1 and C2/A2. Pink data points represent
716 female data while blue data points represent male data. (C) Quantification of the percentage of
717 Vglut3-coexpressing NA neurons among NA neurons in each NA nuclei. Pink data points represent
718 female data while blue data points represent male data. (D) Fluorescent expression of tdTomato
719 (red) and eGFP (green) in coronal sections of Vglut1, Vglut2, or Vglut3 intersectional reporter
720 lines in brainstem NA nuclei. Nucleus is labeled by DAPI (blue). Scale bar 50µm.
721

722 **Figure 2. Characterization of real time co-expression of Vglut1, Vglut2 and Vglut3 in brainstem**
723 **NA neurons in adult mice by fluorescent *in situ* hybridization.** (A) Representative images of
724 *Slc17a7* (Vglut1), *Slc17a6* (Vglut2), and *Slc17a8* (Vglut3) and *Dbh* (DBH) double ISH in coronal
725 sections of WT mice in all of brainstem NA nuclei in adult mice. DBH (green), Vglut1/2/3 (red),
726 DAPI (cyan). Scale bar 50µm. (B) Quantification of the percentage of *Slc17a6* (Vglut2) co-
727 expression in NA neurons in each NA nuclei. Female data (pink), male data (blue). (C)
728 Quantification of the percentage of *Slc17a8* (Vglut3) co-expression in NA neurons in each NA
729 nuclei. Female data (pink), male data (blue).
730
731 **Figure 3. DBH with Vglut2 co-staining by fluorescent *in situ* hybridization confirms that Vglut2**
732 **expression is disrupted in the whole central NA system in Dbh-Cre; Vglut2 cKO mice.** (A)
733 Representative images of *Slc17a6* (Vglut2) and *Dbh* (DBH) double ISH in anterior C1/A1, posterior
734 C1/A1, anterior C2/A2 and posterior C2/A2 in control and Dbh-Cre; Vglut2 cKO mice. DBH (green),
735 Vglut2 (red), DAPI (cyan). Scale bar 20µm.(B) Quantification of intensity of *Slc17a6* (Vglut2) signal
736 in control and Dbh-Cre; Vglut2 cKO mice.
737
738 **Figure 4. Vglut2 conditional knockout in central noradrenergic neurons fails to alter baseline**
739 **breathing and the hypercapnic ventilatory reflex (5% CO_2).** (A) Mouse model schematic and
740 experimental protocol including habituation and hypercapnia protocol (5% CO_2). (B) Under both
741 room air and hypercapnia (5% CO_2), Dbh-Cre; Vglut2 cKO mice didn't show significant changes in
742 respiratory output (V_E/V_{O2}), minute ventilation (V_E), respiratory rate (V_f), tidal volume (V_T),
743 metabolism demand (V_{O2}), inspiratory duration (T_I), expiratory duration (T_E), breath cycle
744 duration (T_{TOT}), inspiratory flow rate (V_T/T_I), and expiratory flow rate (V_T/T_E). Linear mixed-effects
745 regression model, ****$p<0.0001$, **$p<0.01$, *$p<0.05$, ns: $p\geq0.05$.
746
747 **Figure 5. Vglut2 conditional knockout in central noradrenergic neurons fails to alter the**
748 **majority of hypercapnic ventilation parameters and metabolism under 7% CO_2.** (A) Mouse
749 model schematic and experimental protocol including habituation and hypercapnia protocol (7%
750 CO_2). (B) Knocking out Vglut2 in the whole NA system failed to alter V_E/V_{O2}, V_f, V_E, V_{O2}, T_I, T_E, T_{TOT},

751 V_T/T_E but only showed a significantly reduce in V_T and V_T/T_I under 7% CO_2 condition. Linear mixed-
752 effects regression model, ****p<0.0001, **p<0.01, *p<0.05, ns: p≥0.05.
753
754 **Figure 6. Vglut2 conditional knockout in central noradrenergic neurons fails to alter the**
755 **hypercapnic ventilatory reflex (10% CO_2).** (A) Mouse model schematic and experimental
756 protocol including habituation and hypercapnia protocol (10% CO_2). (B) Knocking out Vglut2 in
757 the whole NA system didn't significantly alter V_E/V_{O2}, V_f, V_T, V_E, V_{O2}, T_I, T_E, T_{TOT}, V_T/T_I, and V_T/T_E
758 under 10% CO_2 condition. Linear mixed-effects regression model, ****p<0.0001, **p<0.01,
759 *p<0.05, ns: p≥0.05.
760
761 **Figure 7. Vglut2 conditional knockout in central noradrenergic neurons fails to alter the hypoxic**
762 **ventilatory reflex (10% O_2).** (A) Mouse model schematic and experimental protocol including
763 habituation and hypoxia protocol (10% O_2). (B) Knocking out Vglut2 in the whole NA system did
764 not show significant breathing changes including V_E/V_{O2}, V_E, V_f, V_T, V_{O2}, T_I, T_E, T_{TOT}, V_T/T_I, and V_T/T_E
765 in either of the three five-minute time periods under hypoxia (10% O_2). Linear mixed-effects
766 regression model, ****p<0.0001, **p<0.01, *p<0.05, ns: p≥0.05.
767
768 **Figure 1 Supplement 1. Cumulative fate maps of glutamate co-expressing NA neurons in C3 NA**
769 **nucleus.** (A) Fluorescent expression of tdTomato (red) and eGFP (green) in coronal sections of
770 Vglut1, Vglut2, or Vglut3 intersectional reporter lines in C3 NA nucleus. Nucleus is labeled by DAPI
771 (blue). Scale bar 50µm. (B) Quantification of the percentage of Vglut2 or Vglut3-coexpressing NA
772 neurons among NA neurons in C3 NA nucleus. Female data (pink), male data (blue).
773
774 **Figure 2 Supplement 1. Virus injection of Cre-dependent tdTomato into LC of *Slc17a6^{Cre}* mice.**
775 TH (green), tdTomato (red), nuclei (DAPI). Scale bar 50µm.
776
777 **Figure 2 Supplement 2. Characterization of real time co-expression of Vglut1, Vglut2 and Vglut3**
778 **in C3 NA neurons in adult mice by fluorescent *in situ* hybridization.** (A) Representative images
779 of *Slc17a7* (Vglut1), *Slc17a6* (Vglut2), and *Slc17a8* (Vglut3) and *Dbh* (DBH) double ISH in coronal
780 sections of WT mice in C3 NA nuclei in adult mice. DBH (green), Vglut1/2/3 (red), DAPI (cyan).

781 Scale bar 50µm. (B) Quantification of the percentage of *Slc17a6* (Vglut2)/*Slc17a8* (Vglut3) co-
782 expression in C3 NA nucleus. Female data (pink), male data (blue).
783
784 **Figure 3 Supplement 1. DBH with Vglut2 co-staining by fluorescent *in situ* hybridization**
785 **confirms that Vglut2 expression is disrupted in C3 NA nucleus in Dbh-Cre; Vglut2 cKO mice.** DBH
786 (green), Vglut2 (red), DAPI (cyan). Scale bar 20µm.
787
788 **Figure 4 Supplement 1. Characterization of dynamic patterns of breathing in Dbh-Cre; Vglut2**
789 **cKO mice under room air and hypercapnia (5% CO_2).** Poincaré plots and the measurement of
790 SD1 and SD2 of inspiratory duration (T_I) (A), expiratory duration (T_E) (B), breath cycle duration
791 (T_{TOT}) (C), inspiratory flow rate (V_T/T_I) (D), expiratory flow rate (V_T/T_E) (E), respiratory rate (V_f) (F),
792 tidal volume (V_T) (G), and minute ventilation (V_E) (H) in Dbh-Cre; Vglut2 cKO mice and their
793 littermate controls under room air and 5% CO_2 challenge. Mann-Whitney U test, ns: $p \geq 0.05$, p
794 value was shown if $p<0.05$.
795
796 **Figure 5 Supplement 1. Characterization of dynamic patterns of breathing in Dbh-Cre; Vglut2**
797 **cKO mice under room air and hypercapnia (7% CO_2).** Poincaré plots and the measurement of
798 SD1 and SD2 of T_I (A), T_E (B), T_{TOT} (C), V_T/T_I (D), V_T/T_E (E), V_f (F), V_T (G), and V_E (H) in Dbh-Cre; Vglut2
799 cKO mice and their littermate controls under room air and 7% CO_2 challenge. Mann-Whitney U
800 test, ns: $p \geq 0.05$, p value was shown if $p<0.05$.
801
802 **Figure 6 Supplement 1. Characterization of dynamic patterns of breathing in Dbh-Cre; Vglut2**
803 **cKO mice under room air and hypercapnia (10% CO_2).** Poincaré plots and the measurement of
804 SD1 and SD2 of T_I (A), T_E (B), T_{TOT} (C), V_T/T_I (D), V_T/T_E (E), V_f (F), V_T (G), and V_E (H) in Dbh-Cre; Vglut2
805 cKO mice and their littermate controls under room air and 10% CO_2 challenge. Mann-Whitney U
806 test, ns: $p \geq 0.05$, p value was shown if $p<0.05$.
807 **Figure 7 Supplement 1. Characterization of dynamic patterns of breathing in Dbh-Cre; Vglut2**
808 **cKO mice under room air and hypoxia (10% O_2).** Poincaré plots and the measurement of SD1
809 and SD2 of T_I (A), T_E (B), T_{TOT} (C), V_T/T_I (D), V_T/T_E (E), V_f (F), V_T (G), and V_E (H) in Dbh-Cre; Vglut2

810 cKO mice and their littermate controls under room air and 10% O_2 challenge. Mann-Whitney U
811 test, ns: $p \geq 0.05$, p value was shown if $p<0.05$.

812 **Table 1.** Respiratory and metabolic values under room air conditions and the statistical tests.

813 **Table 2.** Respiratory and metabolic values under 5% CO_2 conditions and the statistical tests.

814 **Table 3.** Respiratory and metabolic values under 7% CO_2 conditions and the statistical tests.

815 **Table 4.** Respiratory and metabolic values under 10% CO_2 conditions and the statistical tests.

816 **Table 5.** Respiratory and metabolic values under 10% O_2 conditions and the statistical tests.

817 **Supplemental table 1.** Vglut2 positive innervations from central noradrenergic neurons to the
818 brain nuclei important in breathing control.

819
820 **References**
821

822 Abbott SBG, DePuy SD, Nguyen T, Coates MB, Stornetta RL, Guyenet PG. 2013. Selective
823 optogenetic activation of rostral ventrolateral medullary catecholaminergic neurons
824 produces cardiorespiratory stimulation in conscious mice. *J Neurosci* **33**:3164–3177.
825 doi:10.1523/JNEUROSCI.1046-12.2013
826 Abbott SBG, Holloway BB, Viar KE, Guyenet PG. 2014. Vesicular glutamate transporter 2 is
827 required for the respiratory and parasympathetic activation produced by optogenetic
828 stimulation of catecholaminergic neurons in the rostral ventrolateral medulla of mice in vivo.
829 *Eur J Neurosci* **39**:98–106. doi:10.1111/ejn.12421
830 Beltrán-Castillo S, Olivares MJ, Contreras RA, Zúñiga G, Llona I, von Bernhardi R, Eugenín JL.
831 2017. D-serine released by astrocytes in brainstem regulates breathing response to CO2
832 levels. *Nat Commun* **8**:838. doi:10.1038/s41467-017-00960-3
833 Chigr F, Najimi M, Jordan D, Denoroy L, Pearson J, Tommasi M, Gilly R, Kopp N. 1989.
834 [Immunohistochemical absence of adrenergic neurons in the dorsal part of the solitary tract
835 nucleus in sudden infant death]. *C R Acad Sci III, Sci Vie* **309**:543–549.
836 Comer AM, Qi J, Christie DL, Gibbons HM, Lipski J. 1998. Noradrenaline transporter expression
837 in the pons and medulla oblongata of the rat: localisation to noradrenergic and some C1
838 adrenergic neurones. *Brain Res Mol Brain Res* **62**:65–76. doi:10.1016/s0169-328x(98)00241-1
839 Del Negro CA, Funk GD, Feldman JL. 2018. Breathing matters. *Nat Rev Neurosci* **19**:351–367.
840 doi:10.1038/s41583-018-0003-6
841 DePuy SD, Stornetta RL, Bochorishvili G, Deisseroth K, Witten I, Coates M, Guyenet PG. 2013.
842 Glutamatergic neurotransmission between the C1 neurons and the parasympathetic
843 preganglionic neurons of the dorsal motor nucleus of the vagus. *J Neurosci* **33**:1486–1497.
844 doi:10.1523/JNEUROSCI.4269-12.2013

845 Dick TE, Dutschmann M, Feldman JL, Fong AY, Hülsmann S, Morris KM, Ramirez JM, Smith JC,
846 Respiratory Neurobiology Consortium. 2018. Facts and challenges in respiratory
847 neurobiology. *Respir Physiol Neurobiol* **258**:104–107. doi:10.1016/j.resp.2015.01.014
848 Ducros L, Vahedi K, Similowski T, Bousser M-G, Payen D. 2003. Uncontrollable high-frequency
849 tachypnea in a case of unilateral medial medullary infarct. *Intensive Care Med* **29**:841–844.
850 doi:10.1007/s00134-003-1658-6
851 Feldman JL, Del Negro CA, Gray PA. 2013. Understanding the rhythm of breathing: so near, yet
852 so far. *Annu Rev Physiol* **75**:423–452. doi:10.1146/annurev-physiol-040510-130049
853 Ferreira CB, Silva TM, Silva PE, Castro CL, Czeisler C, Otero JJ, Takakura AC, Moreira TS. 2022.
854 Phox2b mutation mediated by Atoh1 expression impaired respiratory rhythm and ventilatory
855 responses to hypoxia and hypercapnia. *eLife* **11**. doi:10.7554/eLife.73130
856 Fremeau RT, Voglmaier S, Seal RP, Edwards RH. 2004. VGLUTs define subsets of excitatory
857 neurons and suggest novel roles for glutamate. *Trends Neurosci* **27**:98–103.
858 doi:10.1016/j.tins.2003.11.005
859 Garcia AJ, Koschnitzky JE, Ramirez J-M. 2013. The physiological determinants of sudden infant
860 death syndrome. *Respir Physiol Neurobiol* **189**:288–300. doi:10.1016/j.resp.2013.05.032
861 Gauda EB, Cristofalo E, Nunez J. 2007. Peripheral arterial chemoreceptors and sudden infant
862 death syndrome. *Respir Physiol Neurobiol* **157**:162–170. doi:10.1016/j.resp.2007.02.016
863 Guyenet PG, Stornetta RL, Bochorishvili G, Depuy SD, Burke PGR, Abbott SBG. 2013. C1
864 neurons: the body's EMTs. *Am J Physiol Regul Integr Comp Physiol* **305**:R187-204.
865 doi:10.1152/ajpregu.00054.2013
866 Haxhiu MA, Yung K, Erokwu B, Cherniack NS. 1996. CO2-induced c-fos expression in the CNS
867 catecholaminergic neurons. *Respir Physiol* **105**:35–45. doi:10.1016/0034-5687(96)00034-5
868 Henneberger C, Bard L, Panatier A, Reynolds JP, Kopach O, Medvedev NI, Minge D, Herde MK,
869 Anders S, Kraev I, Heller JP, Rama S, Zheng K, Jensen TP, Sanchez-Romero I, Jackson CJ,
870 Janovjak H, Ottersen OP, Nagelhus EA, Oliet SHR, Stewart MG, Nägerl UV, Rusakov DA. 2020.
871 LTP induction boosts glutamate spillover by driving withdrawal of perisynaptic astroglia.
872 *Neuron* **108**:919-936.e11. doi:10.1016/j.neuron.2020.08.030
873 Hülsmann S, Oku Y, Zhang W, Richter DW. 2000. Metabotropic glutamate receptors and
874 blockade of glial Krebs cycle depress glycinergic synaptic currents of mouse hypoglossal
875 motoneurons. *Eur J Neurosci* **12**:239–246.
876 Kopp N, Chigr F, Denoroy L, Gilly R, Jordan D. 1993. Absence of adrenergic neurons in nucleus
877 tractus solitarius in sudden infant death syndrome. *Neuropediatrics* **24**:25–29. doi:10.1055/s-
878 2008-1071508
879 Lorang D, Amara SG, Simerly RB. 1994. Cell-type-specific expression of catecholamine
880 transporters in the rat brain. *J Neurosci* **14**:4903–4914. doi:10.1523/JNEUROSCI.14-08-
881 04903.1994
882 Lusk S, Ward CS, Chang A, Twitchell-Heyne A, Fattig S, Allen G, Jankowsky JL, Ray RS. 2023. An
883 automated respiratory data pipeline for waveform characteristic analysis. *J Physiol (Lond)*
884 **601**:4767–4806. doi:10.1113/JP284363
885 Malheiros-Lima MR, Silva JN, Souza FC, Takakura AC, Moreira TS. 2020. C1 neurons are part of
886 the circuitry that recruits active expiration in response to the activation of peripheral
887 chemoreceptors. *eLife* **9**. doi:10.7554/eLife.52572

Malheiros-Lima MR, Silva TM, Takakura AC, Moreira TS. 2022. A5 noradrenergic-projecting C1 neurons activate sympathetic and breathing outputs in anaesthetized rats. *Exp Physiol* **107**:147–160. doi:10.1113/EP089691

Malheiros-Lima MR, Totola LT, Lana MVG, Strauss BE, Takakura AC, Moreira TS. 2018. Breathing responses produced by optogenetic stimulation of adrenergic C1 neurons are dependent on the connection with preBötzinger complex in rats. *Pflugers Arch* **470**:1659–1672. doi:10.1007/s00424-018-2186-0

Mansouri J, Panigrahy A, Filiano JJ, Sleeper LA, St John WM, Kinney HC. 2001. Alpha2 receptor binding in the medulla oblongata in the sudden infant death syndrome. *J Neuropathol Exp Neurol* **60**:141–146.

Martinez VK, Saldana-Morales F, Sun JJ, Zhu PJ, Costa-Mattioli M, Ray RS. 2019. Off-Target Effects of Clozapine-N-Oxide on the Chemosensory Reflex Are Masked by High Stress Levels. *Front Physiol* **10**:521. doi:10.3389/fphys.2019.00521

Ozawa Y, Takashima S, Tada H. 2003. Alpha2-adrenergic receptor subtype alterations in the brainstem in the sudden infant death syndrome. *Early Hum Dev* **75 Suppl**:S129-38. doi:10.1016/j.earlhumdev.2003.08.016

Ramirez J-M, Karlen-Amarante M, Wang J-DJ, Bush NE, Carroll MS, Weese-Mayer DE, Huff A. 2020. The pathophysiology of rett syndrome with a focus on breathing dysfunctions. *Physiology (Bethesda)* **35**:375–390. doi:10.1152/physiol.00008.2020

Ray RS, Corcoran AE, Brust RD, Kim JC, Richerson GB, Nattie E, Dymecki SM. 2011. Impaired respiratory and body temperature control upon acute serotonergic neuron inhibition. *Science* **333**:637–642. doi:10.1126/science.1205295

Robertson SD, Plummer NW, de Marchena J, Jensen P. 2013. Developmental origins of central norepinephrine neuron diversity. *Nat Neurosci* **16**:1016–1023. doi:10.1038/nn.3458

Roux J-C, Dura E, Moncla A, Mancini J, Villard L. 2007. Treatment with desipramine improves breathing and survival in a mouse model for Rett syndrome. *Eur J Neurosci* **25**:1915–1922. doi:10.1111/j.1460-9568.2007.05466.x

Ruohonen ST, Pesonen U, Savontaus E. 2012. Neuropeptide Y in the noradrenergic neurons induces the development of cardiometabolic diseases in a transgenic mouse model. *Indian J Endocrinol Metab* **16**:S569-76. doi:10.4103/2230-8210.105574

Souza GMPR, Stornetta DS, Vitali AJ, Wildner H, Zeilhofer HU, Campbell JN, Abbott SBG. 2022a. Chemogenetic activation of noradrenergic A5 neurons increases blood pressure and visceral sympathetic activity in adult rats. *Am J Physiol Regul Integr Comp Physiol* **323**:R512–R531. doi:10.1152/ajpregu.00119.2022

Souza GMPR, Stornetta RL, Stornetta DS, Guyenet PG, Abbott SBG. 2022b. Adrenergic C1 neurons monitor arterial blood pressure and determine the sympathetic response to hemorrhage. *Cell Rep* **38**:110480. doi:10.1016/j.celrep.2022.110480

Stornetta RL, Sevigny CP, Guyenet PG. 2002a. Vesicular glutamate transporter DNPI/VGLUT2 mRNA is present in C1 and several other groups of brainstem catecholaminergic neurons. *J Comp Neurol* **444**:191–206. doi:10.1002/cne.10141

Stornetta RL, Sevigny CP, Schreihofer AM, Rosin DL, Guyenet PG. 2002b. Vesicular glutamate transporter DNPI/VGLUT2 is expressed by both C1 adrenergic and nonaminergic presympathetic vasomotor neurons of the rat medulla. *J Comp Neurol* **444**:207–220. doi:10.1002/cne.10142

932 Sun JJ, Ray R. 2016. Generation of Two Noradrenergic-Specific Dopamine-Beta-Hydroxylase-
933 FLPo Knock-In Mice Using CRISPR/Cas9-Mediated Targeting in Embryonic Stem Cells. *PLoS*
934 *ONE* **11**:e0159474. doi:10.1371/journal.pone.0159474
935 Takashima S, Becker LE. 1991. Delayed dendritic development of catecholaminergic neurons in
936 the ventrolateral medulla of children who died of sudden infant death syndrome.
937 *Neuropediatrics* **22**:97–99. doi:10.1055/s-2008-1071424
938 Tasan RO, Nguyen NK, Weger S, Sartori SB, Singewald N, Heilbronn R, Herzog H, Sperk G. 2010.
939 The central and basolateral amygdala are critical sites of neuropeptide Y/Y2 receptor-
940 mediated regulation of anxiety and depression. *J Neurosci* **30**:6282–6290.
941 doi:10.1523/JNEUROSCI.0430-10.2010
942 Tong Q, Ye C, McCrimmon RJ, Dhillon H, Choi B, Kramer MD, Yu J, Yang Z, Christiansen LM, Lee
943 CE, Choi CS, Zigman JM, Shulman GI, Sherwin RS, Elmquist JK, Lowell BB. 2007. Synaptic
944 glutamate release by ventromedial hypothalamic neurons is part of the neurocircuitry that
945 prevents hypoglycemia. *Cell Metab* **5**:383–393. doi:10.1016/j.cmet.2007.04.001
946 Viemari J-C, Roux J-C, Tryba AK, Saywell V, Burnet H, Peña F, Zanella S, Bévengut M,
947 Barthelemy-Requin M, Herzing LBK, Moncla A, Mancini J, Ramirez J-M, Villard L, Hilaire G.
948 2005. Mecp2 deficiency disrupts norepinephrine and respiratory systems in mice. *J Neurosci*
949 **25**:11521–11530. doi:10.1523/JNEUROSCI.4373-05.2005
950 Viemari J-C. 2008. Noradrenergic modulation of the respiratory neural network. *Respir Physiol*
951 *Neurobiol* **164**:123–130. doi:10.1016/j.resp.2008.06.016
952 Weinshenker D, Holmes PV. 2016. Regulation of neurological and neuropsychiatric phenotypes
953 by locus coeruleus-derived galanin. *Brain Res* **1641**:320–337.
954 doi:10.1016/j.brainres.2015.11.025
955 Yang B, Sanches-Padilla J, Kondapalli J, Morison SL, Delpire E, Awatramani R, Surmeier DJ. 2021.
956 Locus coeruleus anchors a trisynaptic circuit controlling fear-induced suppression of feeding.
957 *Neuron* **109**:823-838.e6. doi:10.1016/j.neuron.2020.12.023
958 Yang CF, Feldman JL. 2018. Efferent projections of excitatory and inhibitory preBötzinger
959 Complex neurons. *J Comp Neurol* **526**:1389–1402. doi:10.1002/cne.24415
960 Yaylaoglu MB, Titmus A, Visel A, Alvarez-Bolado G, Thaller C, Eichele G. 2005. Comprehensive
961 expression atlas of fibroblast growth factors and their receptors generated by a novel robotic
962 in situ hybridization platform. *Dev Dyn* **234**:371–386. doi:10.1002/dvdy.20441

Figure 1

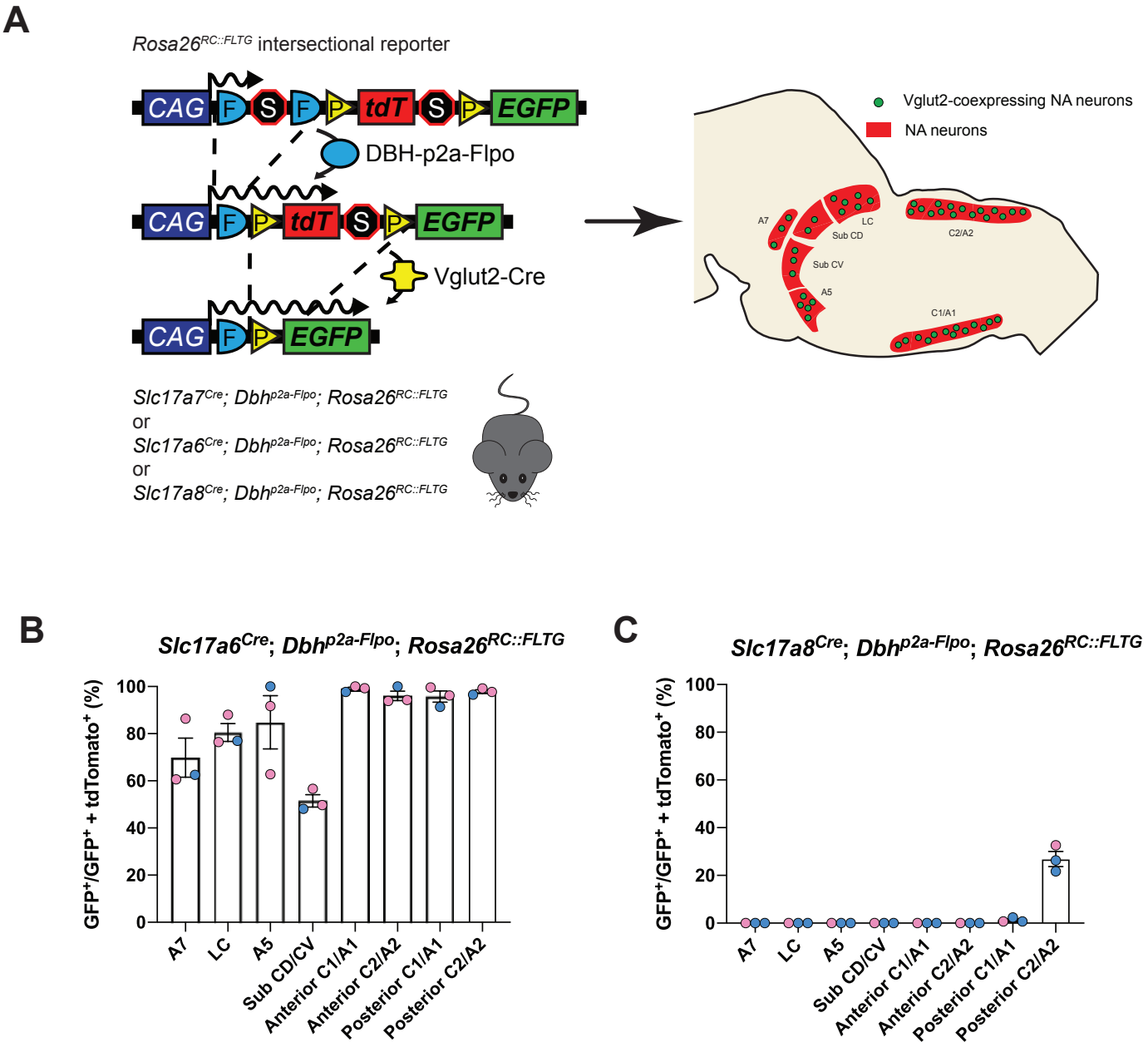
A
Rosa26RC::FLTG intersectional reporter
CAG
F
S
F
P
tdT
S
P
EGFP
DBH-p2a-Flpo
CAG
F
P
tdT
S
P
EGFP
Vglut2-Cre
CAG
F
P
EGFP
Slc17a7Cre; Dbhp2a-Flpo; Rosa26RC::FLTG
or
Slc17a6Cre; Dbhp2a-Flpo; Rosa26RC::FLTG
or
Slc17a8Cre; Dbhp2a-Flpo; Rosa26RC::FLTG
Vglut2-coexpressing NA neurons
NA neurons
A7
LC
Sub CD
C2/A2
Sub CV
A5
C1/A1
B
Slc17a6Cre; Dbhp2a-Flpo; Rosa26RC::FLTG
GFP+/GFP+ + tdTomato+ (%)
100
80
60
40
20
0
A7
LC
A5
Sub CD/CV
Anterior C1/A1
Anterior C2/A2
Posterior C1/A1
Posterior C2/A2
C
Slc17a8Cre; Dbhp2a-Flpo; Rosa26RC::FLTG
GFP+/GFP+ + tdTomato+ (%)
100
80
60
40
20
0
A7
LC
A5
Sub CD/CV
Anterior C1/A1
Anterior C2/A2
Posterior C1/A1
Posterior C2/A2

Figure 1. cont.

D

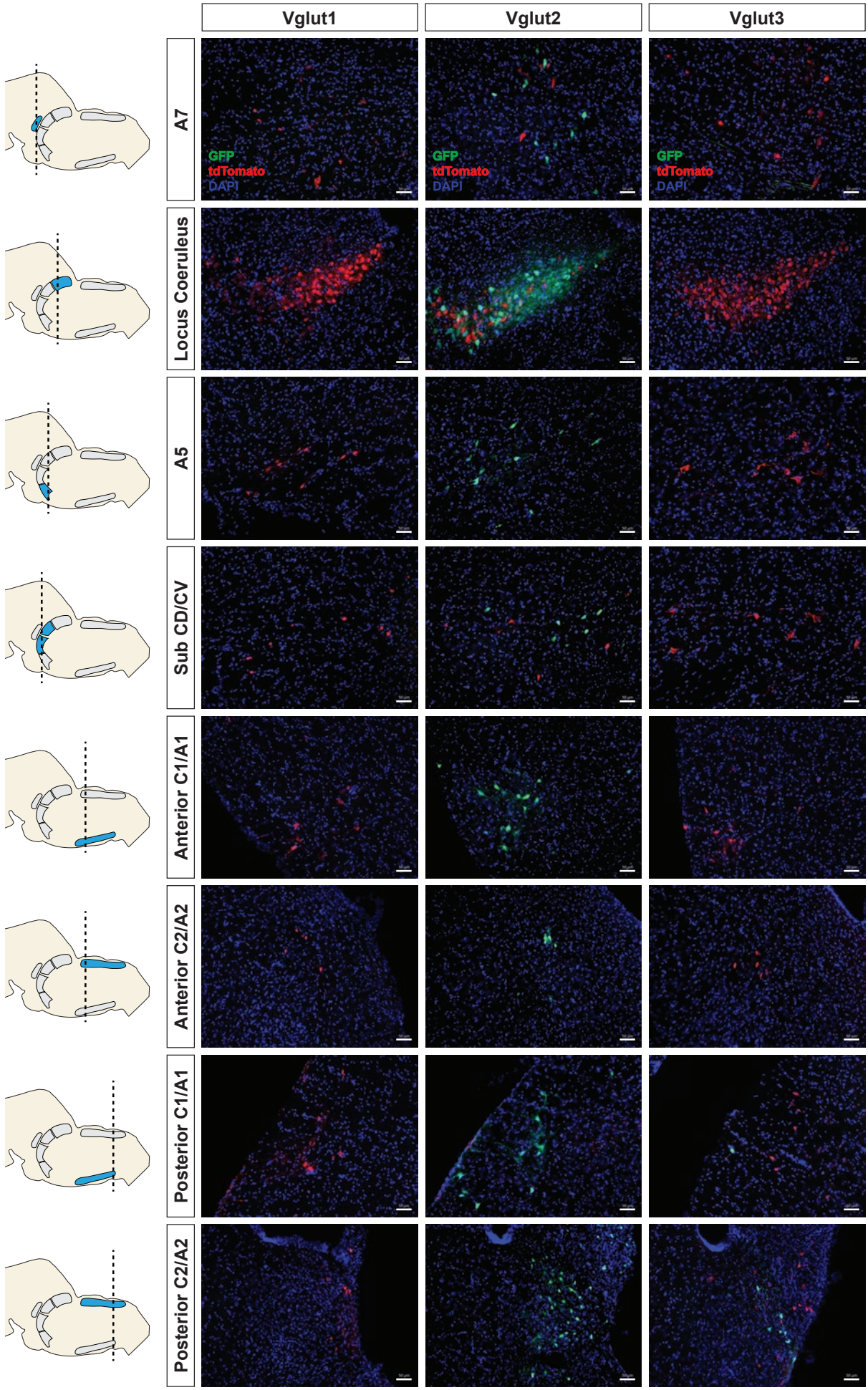

Figure 2

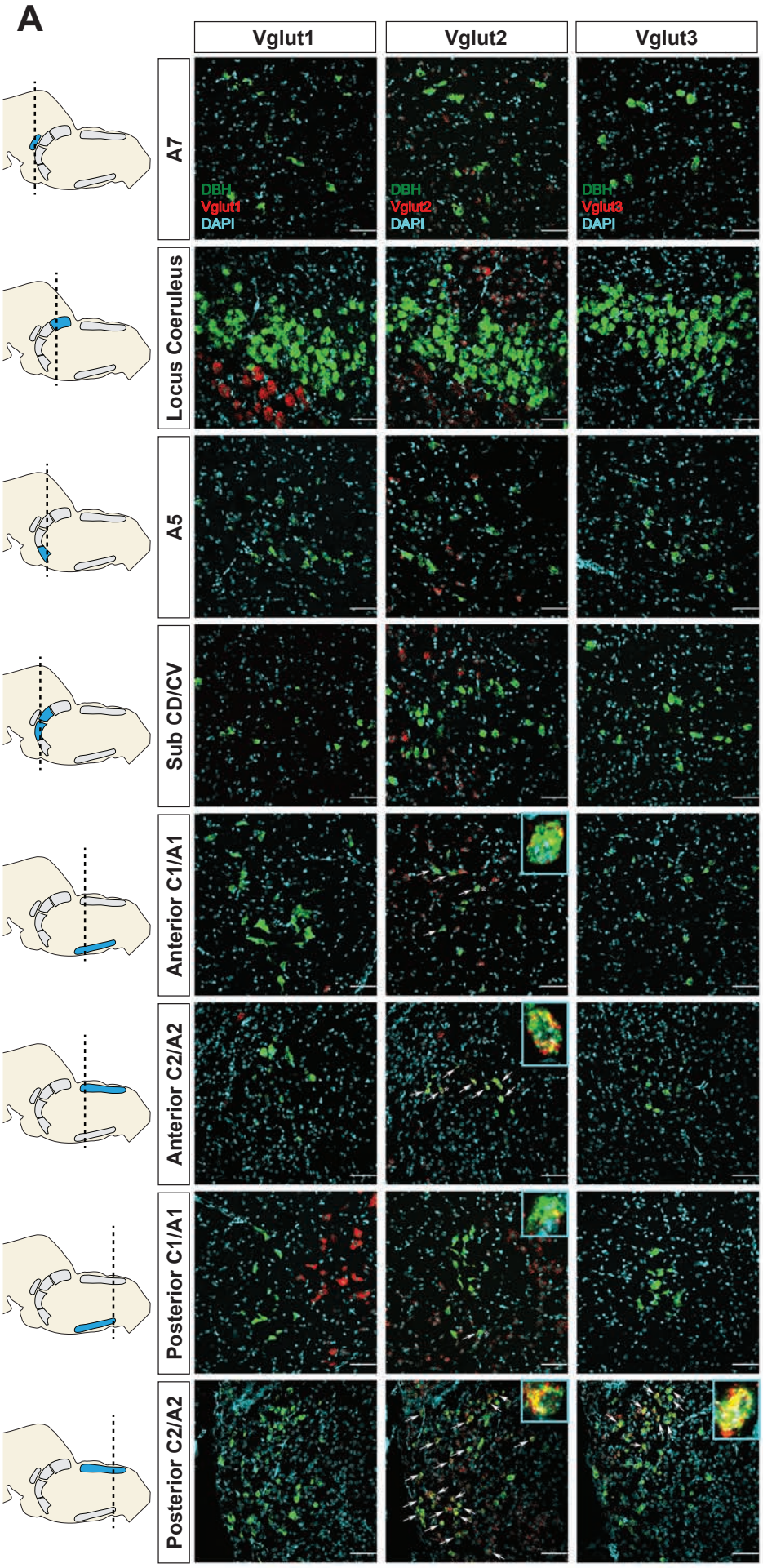
A
Vglut1
Vglut2
Vglut3
A7
Locus Coeruleus
A5
Sub CD/CV
Anterior C1/A1
Anterior C2/A2
Posterior C1/A1
Posterior C2/A2
DBH
Vglut1
DAPI
DBH
Vglut2
DAPI
DBH
Vglut3
DAPI

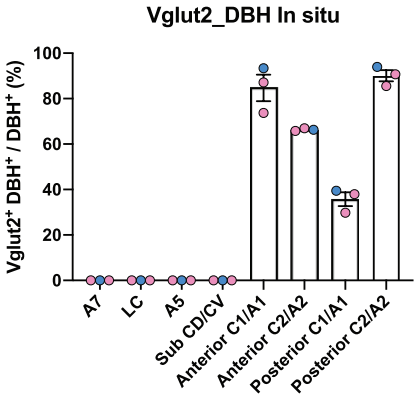
B
Vglut2_DBH In situ
Vglut2+ DBH+ / DBH+ (%)
100
80
60
40
20
0
A7
LC
A5
Sub CD/CV
Anterior C1/A1
Anterior C2/A2
Posterior C1/A1
Posterior C2/A2

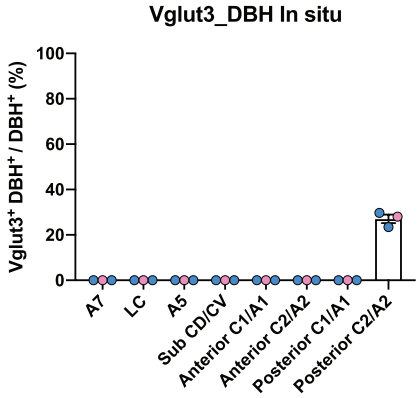
C
Vglut3_DBH In situ
Vglut3+ DBH+ / DBH+ (%)
100
80
60
40
20
0
A7
LC
A5
Sub CD/CV
Anterior C1/A1
Anterior C2/A2
Posterior C1/A1
Posterior C2/A2

Figure 3

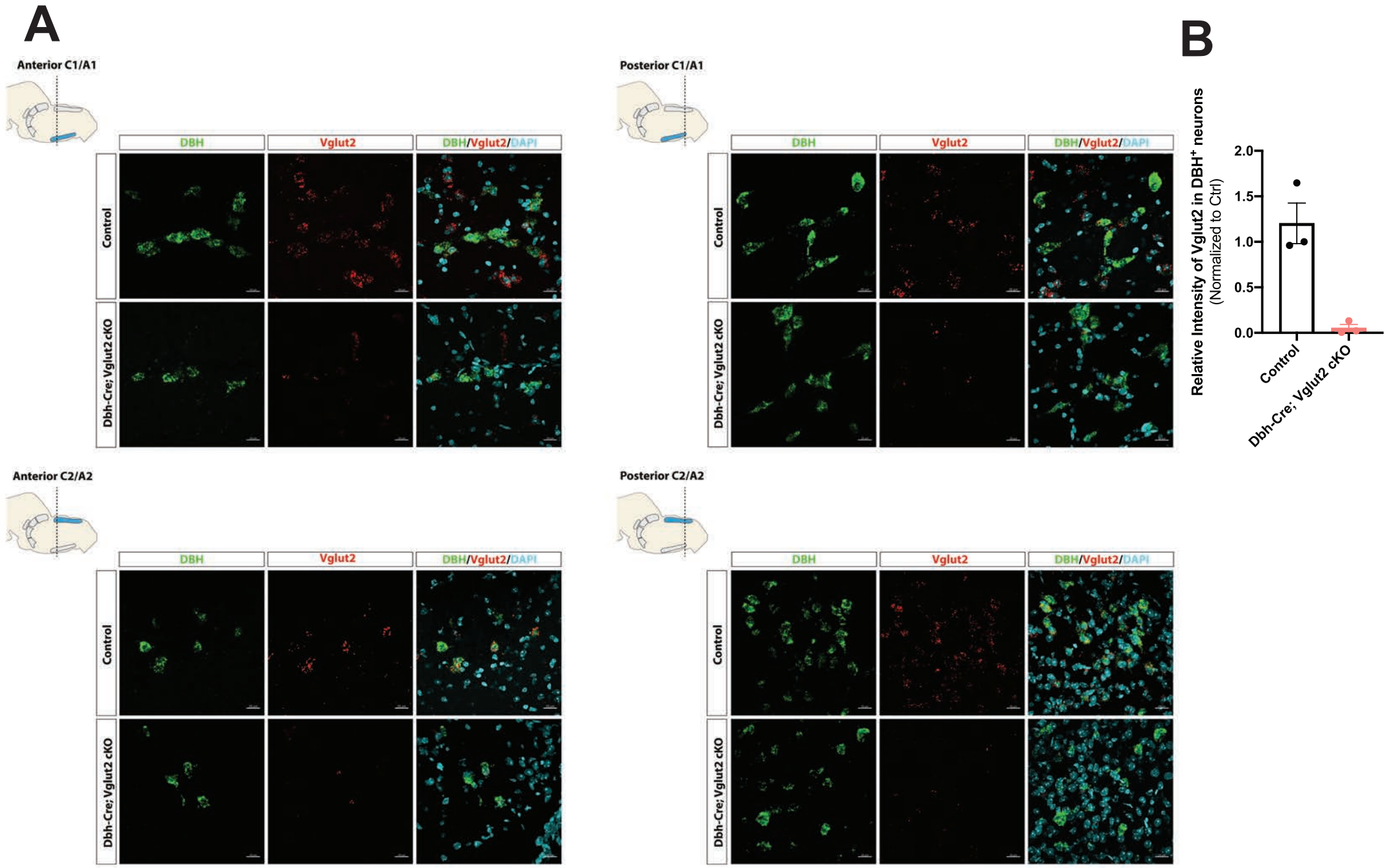
A
Anterior C1/A1
Posterior C1/A1
Anterior C2/A2
Posterior C2/A2
DBH
Vglut2
DBH/Vglut2/DAPI
Control
Dbh-Cre; Vglut2 cKO
B
Relative Intensity of Vglut2 in DBH+ neurons
(Normalized to Ctrl)
2.0
1.5
1.0
0.5
0.0
Control
Dbh-Cre; Vglut2 cKO

Figure 4

A

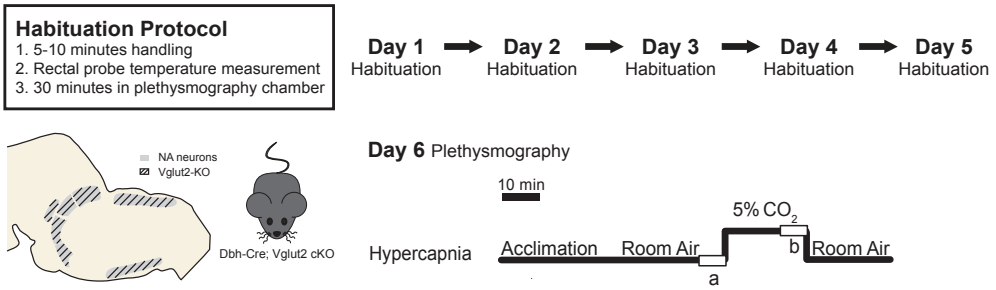
Habituation Protocol
1. 5-10 minutes handling
2. Rectal probe temperature measurement
3. 30 minutes in plethysmography chamber
Day 1 Habituation
Day 2 Habituation
Day 3 Habituation
Day 4 Habituation
Day 5 Habituation
NA neurons
Vglut2-KO
Dbh-Cre; Vglut2 cKO
Day 6 Plethysmography
10 min
Hypercapnia
Acclimation
Room Air
5% CO2
a
b
Room Air

B

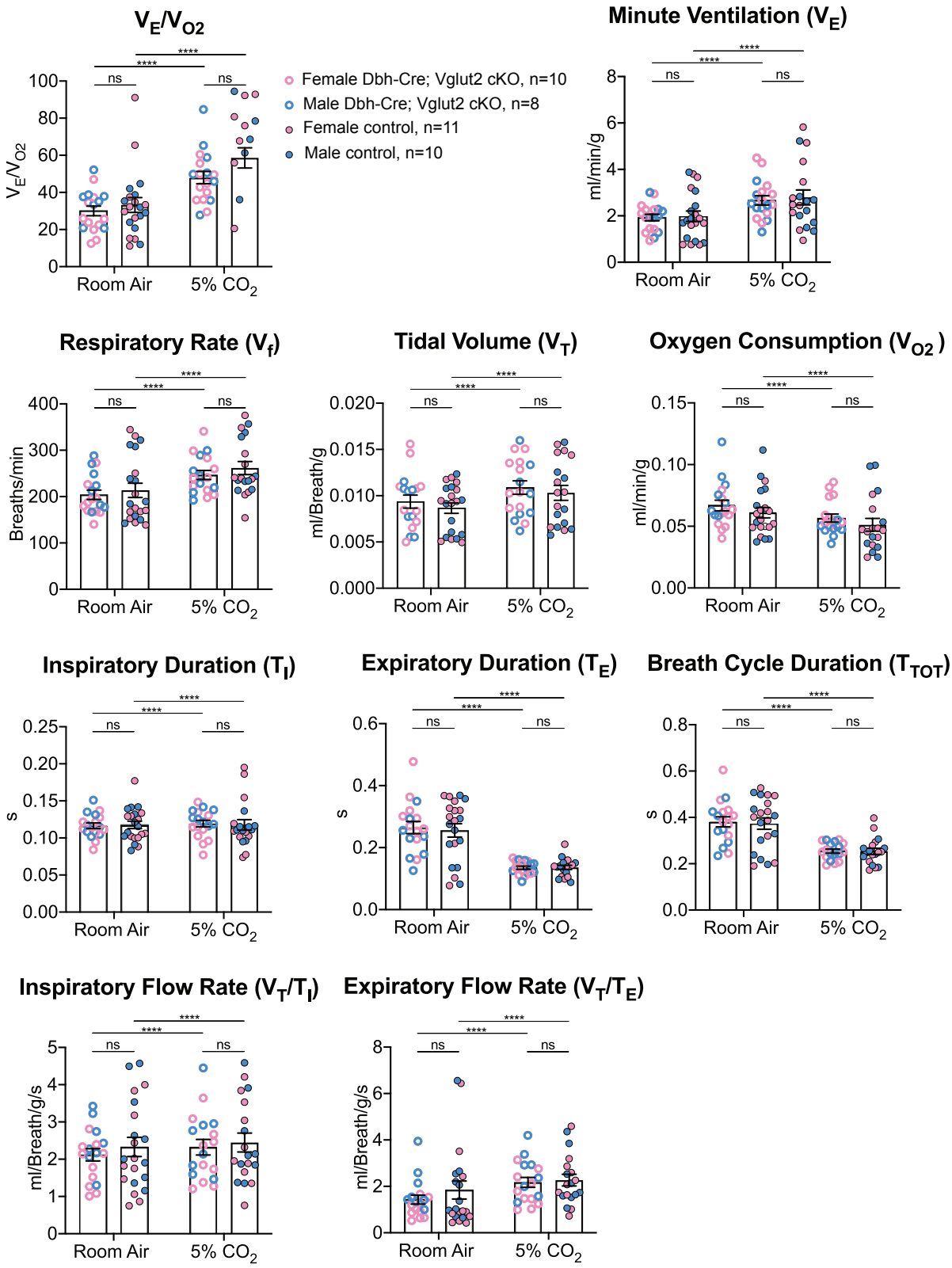
VE/VO2
Minute Ventilation (VE)
Female Dbh-Cre; Vglut2 cKO, n=10
Male Dbh-Cre; Vglut2 cKO, n=8
Female control, n=11
Male control, n=10
Respiratory Rate (Vf)
Tidal Volume (VT)
Oxygen Consumption (VO2)
Inspiratory Duration (TI)
Expiratory Duration (TE)
Breath Cycle Duration (TTOT)
Inspiratory Flow Rate (VT/TI)
Expiratory Flow Rate (VT/TE)
Breaths/min
ml/Breath/g
ml/min/g
ml/Breath/g/s
s
Room Air
5% CO2
ns
****

Figure 5

A

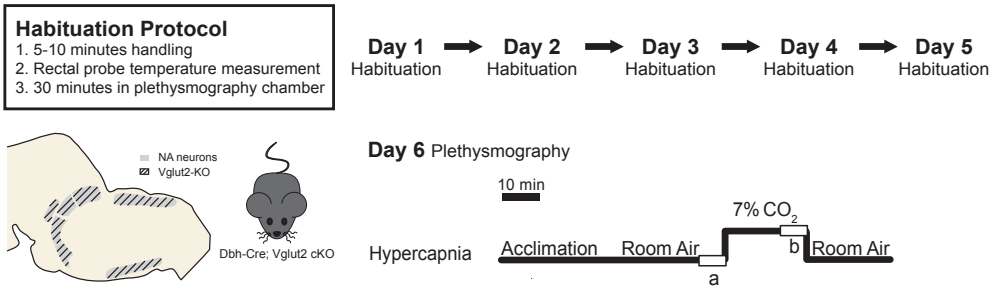
Habituation Protocol
1. 5-10 minutes handling
2. Rectal probe temperature measurement
3. 30 minutes in plethysmography chamber
Day 1 Habituation
Day 2 Habituation
Day 3 Habituation
Day 4 Habituation
Day 5 Habituation
NA neurons
Vglut2-KO
Dbh-Cre; Vglut2 cKO
Day 6 Plethysmography
10 min
Hypercapnia
Acclimation
Room Air
7% CO2
a
b
Room Air

B

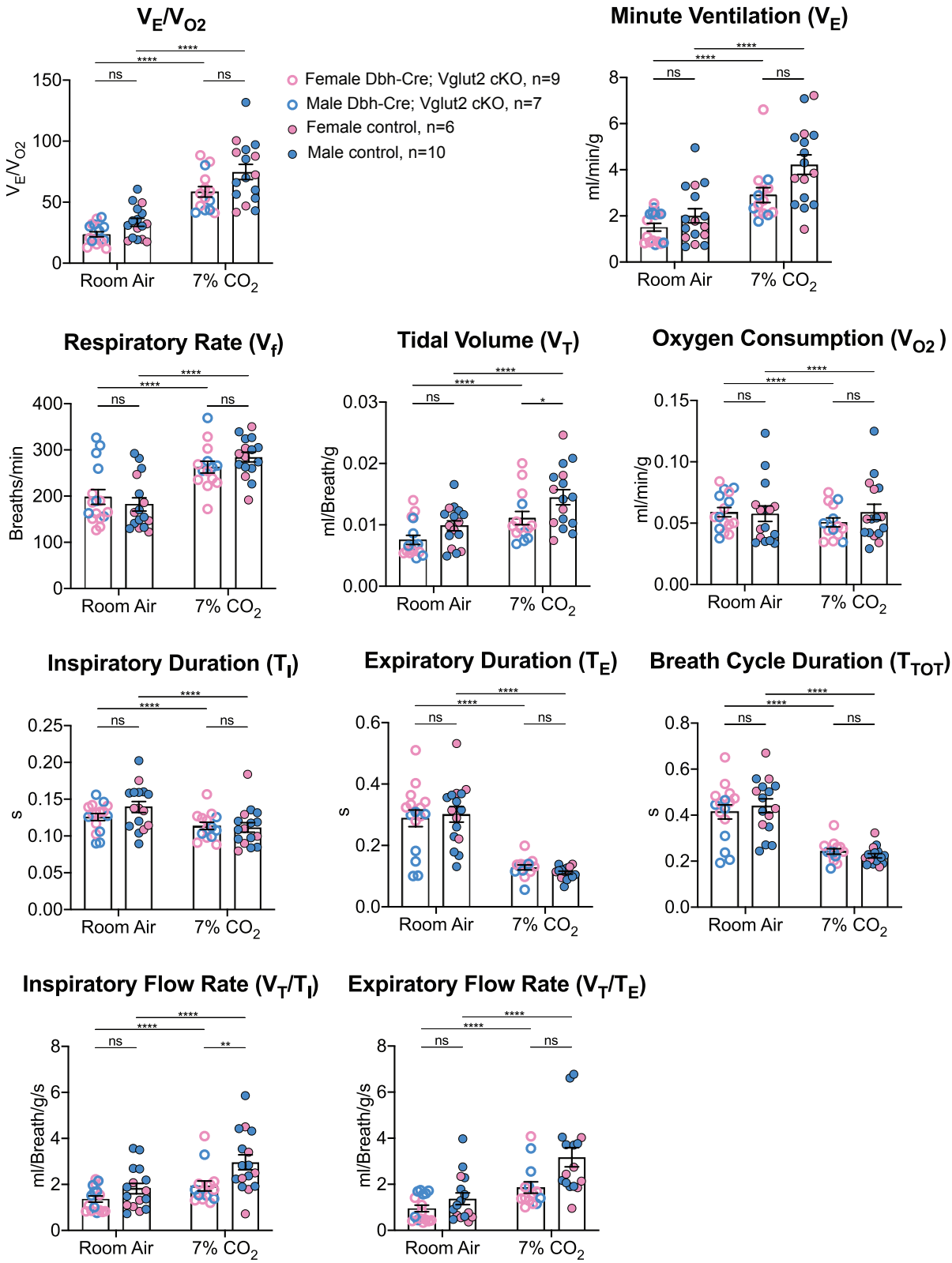
VE/VO2
Minute Ventilation (VE)
Respiratory Rate (Vf)
Tidal Volume (VT)
Oxygen Consumption (VO2)
Inspiratory Duration (TI)
Expiratory Duration (TE)
Breath Cycle Duration (TTOT)
Inspiratory Flow Rate (VT/TI)
Expiratory Flow Rate (VT/TE)
Female Dbh-Cre; Vglut2 cKO, n=9
Male Dbh-Cre; Vglut2 cKO, n=7
Female control, n=6
Male control, n=10
Room Air
7% CO2
ns
****
*
**
ml/min/g
Breaths/min
ml/Breath/g
ml/Breath/g/s
s

Figure 6

A

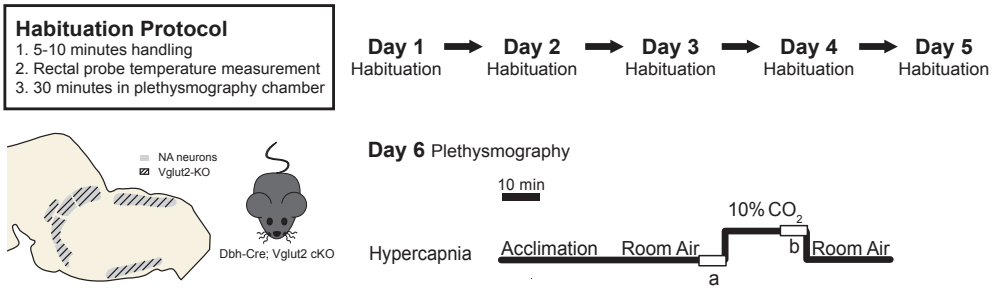
Habituation Protocol
1. 5-10 minutes handling
2. Rectal probe temperature measurement
3. 30 minutes in plethysmography chamber
Day 1 Habituation
Day 2 Habituation
Day 3 Habituation
Day 4 Habituation
Day 5 Habituation
NA neurons
Vglut2-KO
Dbh-Cre; Vglut2 cKO
Day 6 Plethysmography
10 min
Hypercapnia
Acclimation
Room Air
10% CO2
a
b
Room Air

B

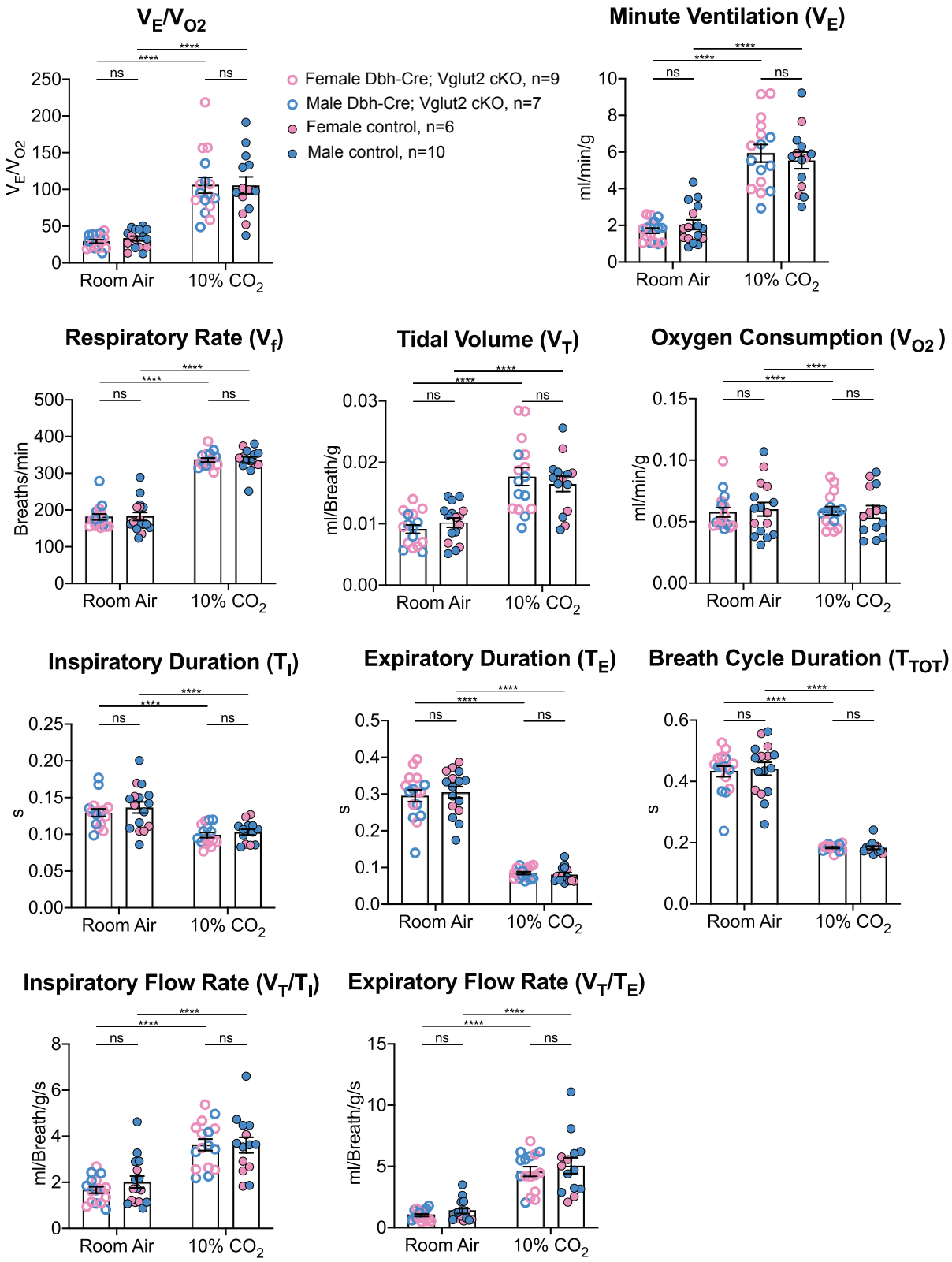
VE/VO2
Minute Ventilation (VE)
Respiratory Rate (Vf)
Tidal Volume (VT)
Oxygen Consumption (VO2)
Inspiratory Duration (TI)
Expiratory Duration (TE)
Breath Cycle Duration (TTOT)
Inspiratory Flow Rate (VT/TI)
Expiratory Flow Rate (VT/TE)
Female Dbh-Cre; Vglut2 cKO, n=9
Male Dbh-Cre; Vglut2 cKO, n=7
Female control, n=6
Male control, n=10
ns
****
Room Air
10% CO2
ml/min/g
Breaths/min
ml/Breath/g
s
ml/Breath/g/s

Figure 7

A

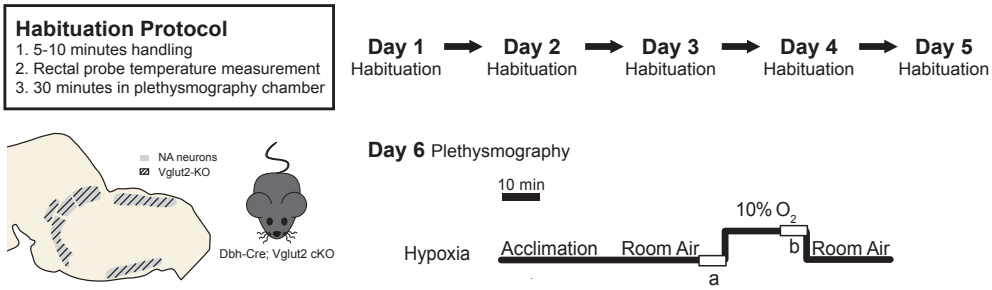
Habituation Protocol
1. 5-10 minutes handling
2. Rectal probe temperature measurement
3. 30 minutes in plethysmography chamber
Day 1 Habituation
Day 2 Habituation
Day 3 Habituation
Day 4 Habituation
Day 5 Habituation
NA neurons
Vglut2-KO
Dbh-Cre; Vglut2 cKO
Day 6 Plethysmography
10 min
Hypoxia
Acclimation
Room Air
10% O2
a
b
Room Air

B

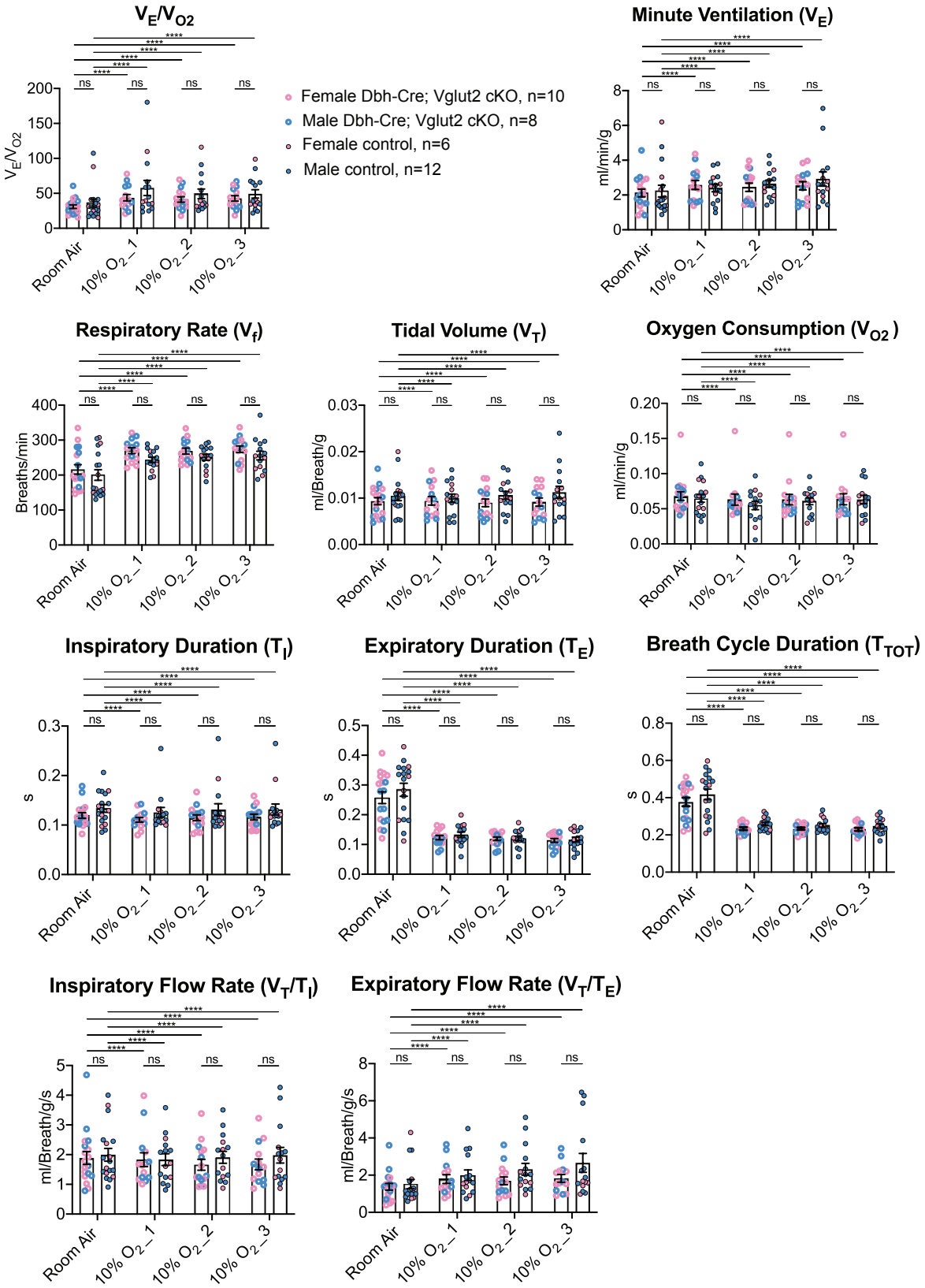
VE/VO2
Minute Ventilation (VE)
Female Dbh-Cre; Vglut2 cKO, n=10
Male Dbh-Cre; Vglut2 cKO, n=8
Female control, n=6
Male control, n=12
Respiratory Rate (Vf)
Tidal Volume (VT)
Oxygen Consumption (VO2)
Inspiratory Duration (TI)
Expiratory Duration (TE)
Breath Cycle Duration (TTOT)
Inspiratory Flow Rate (VT/TI)
Expiratory Flow Rate (VT/TE)
ml/min/g
Breaths/min
ml/Breath/g
ml/Breath/g/s
s
ns
****
Room Air
10% O2_1
10% O2_2
10% O2_3

Figure 1 Supplement 1

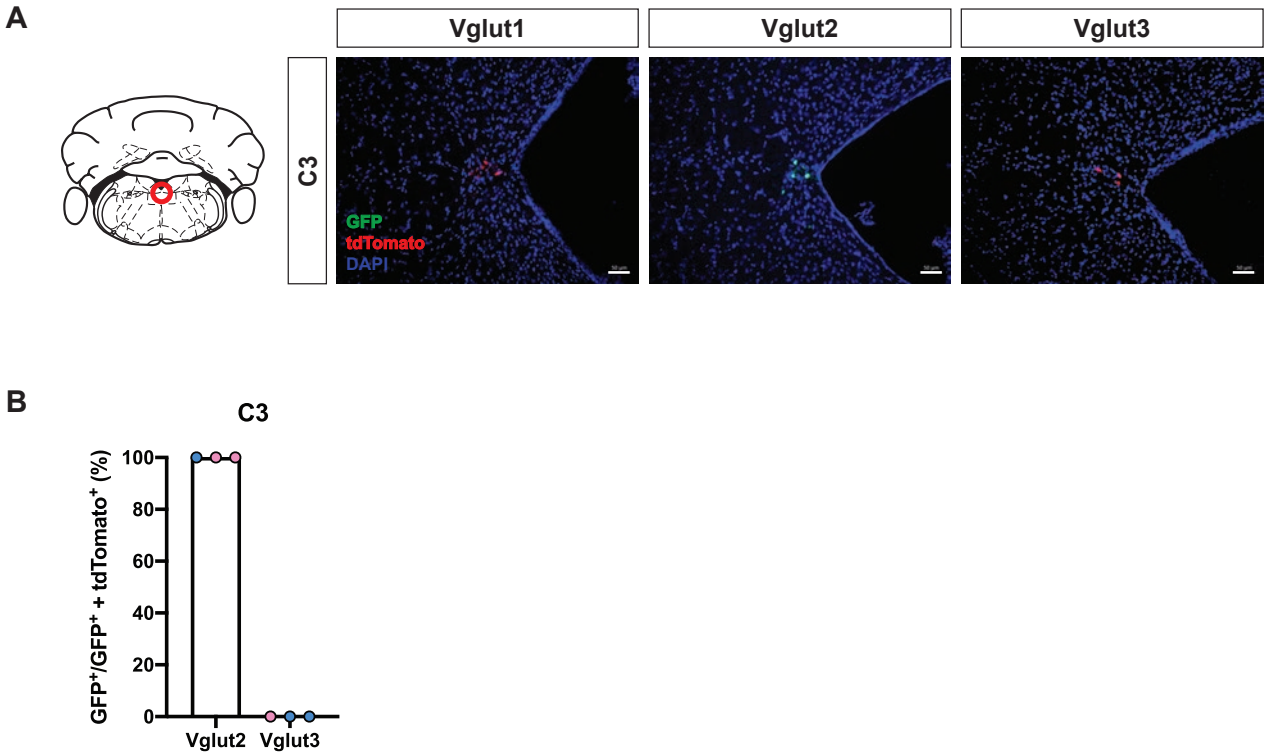

Figure 2 supplement 1

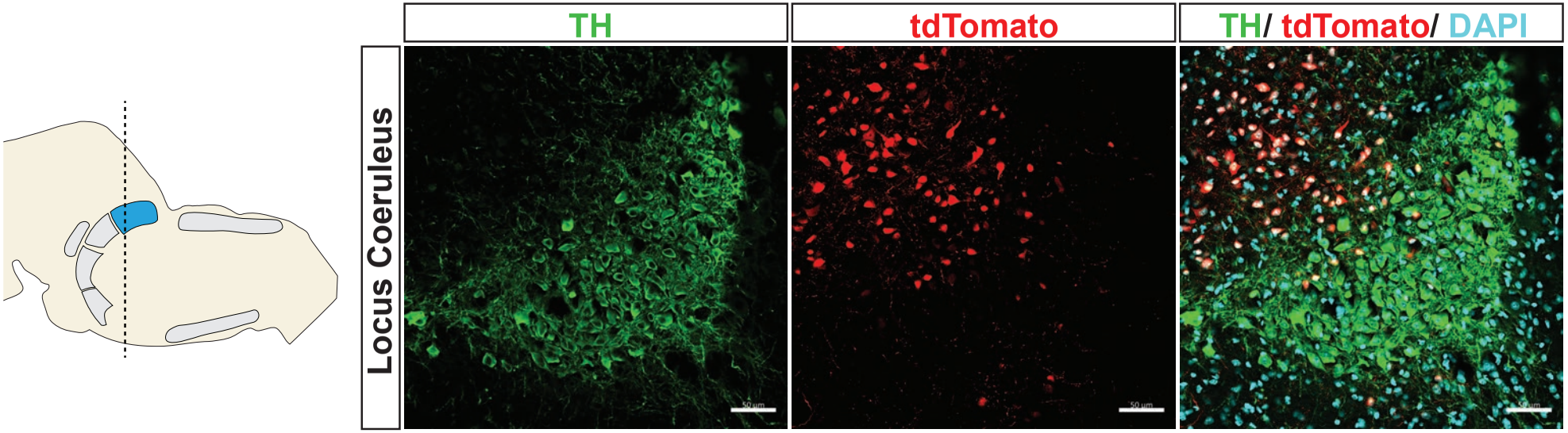

Figure 2 Supplement 2

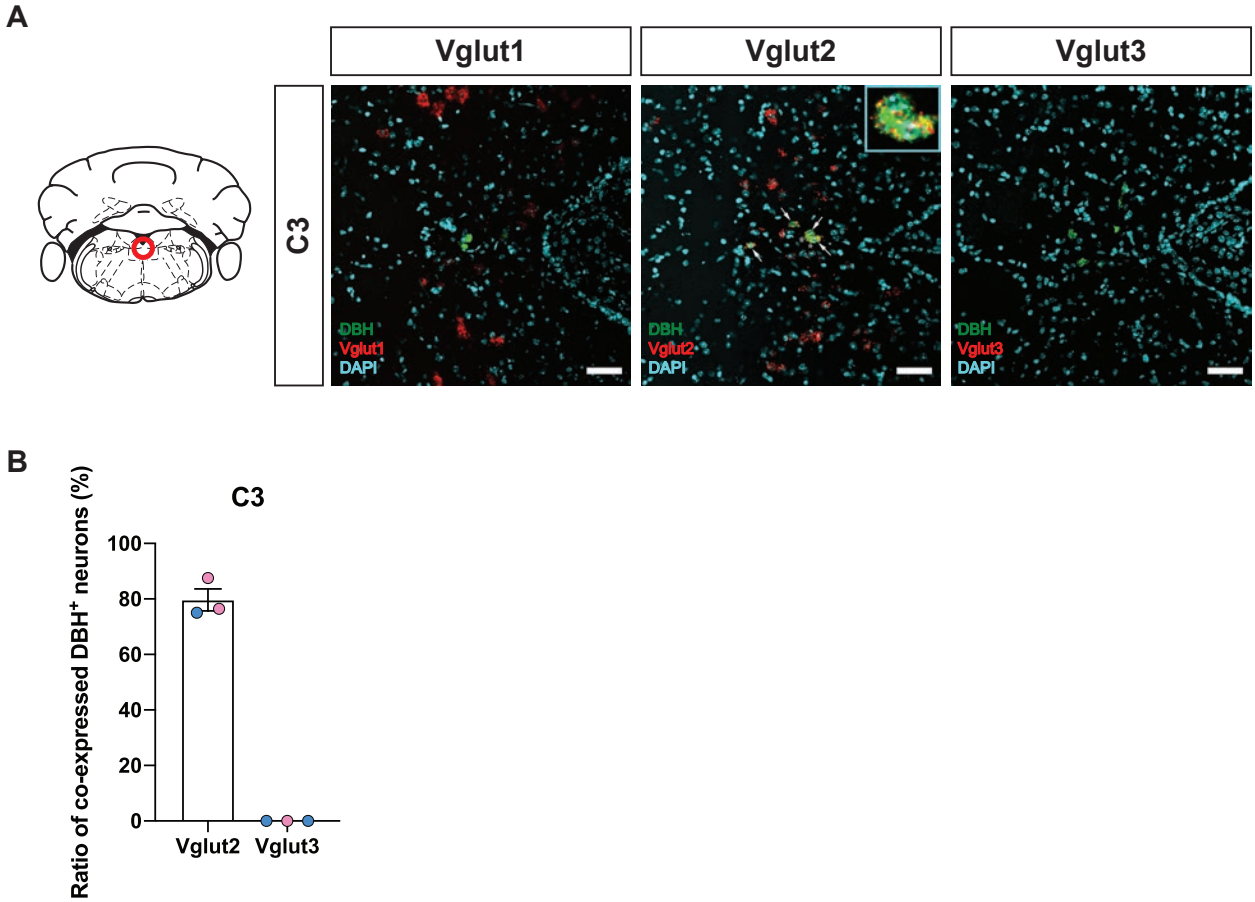

Figure 3 Supplement 1

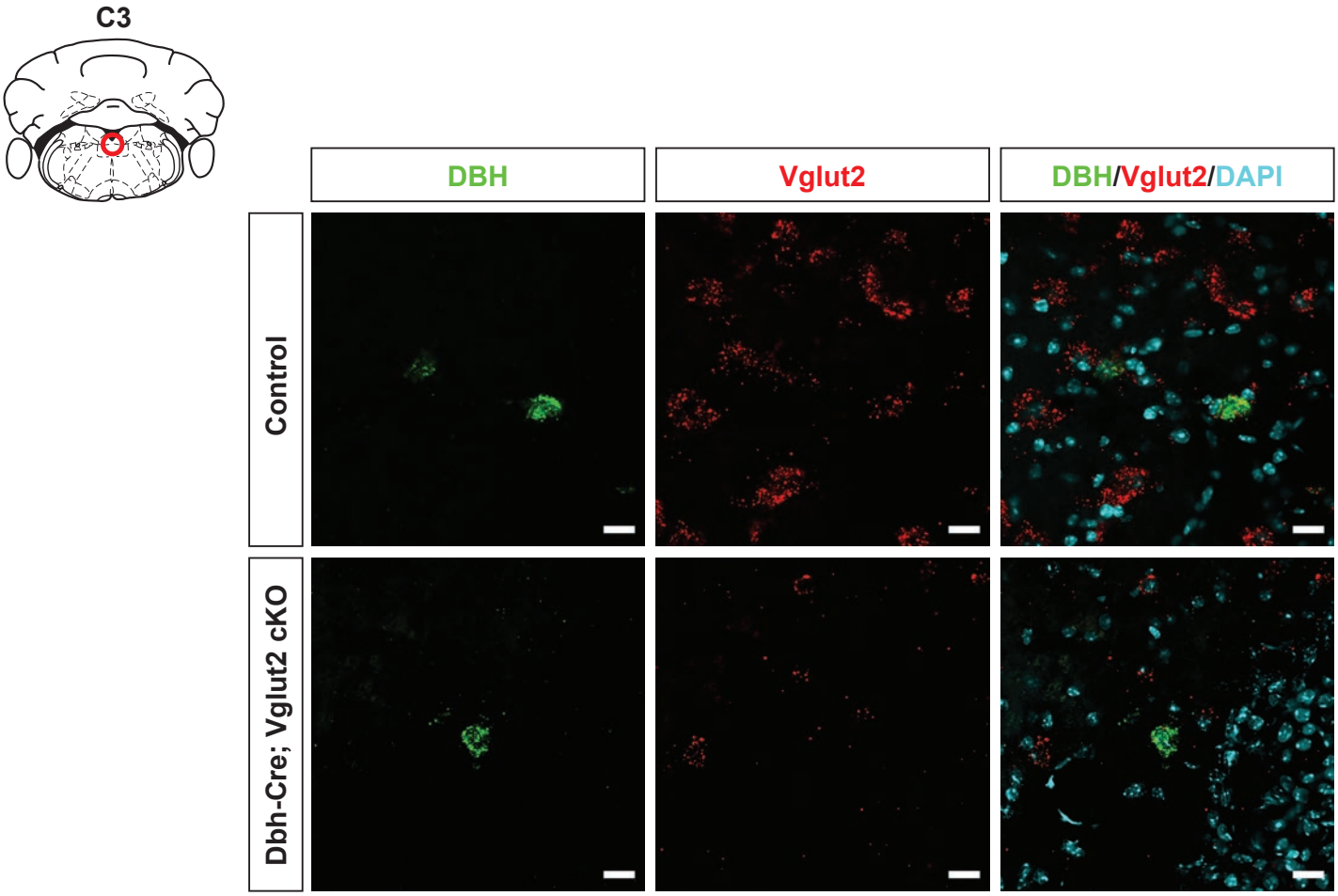

Figure 4 Supplement 1

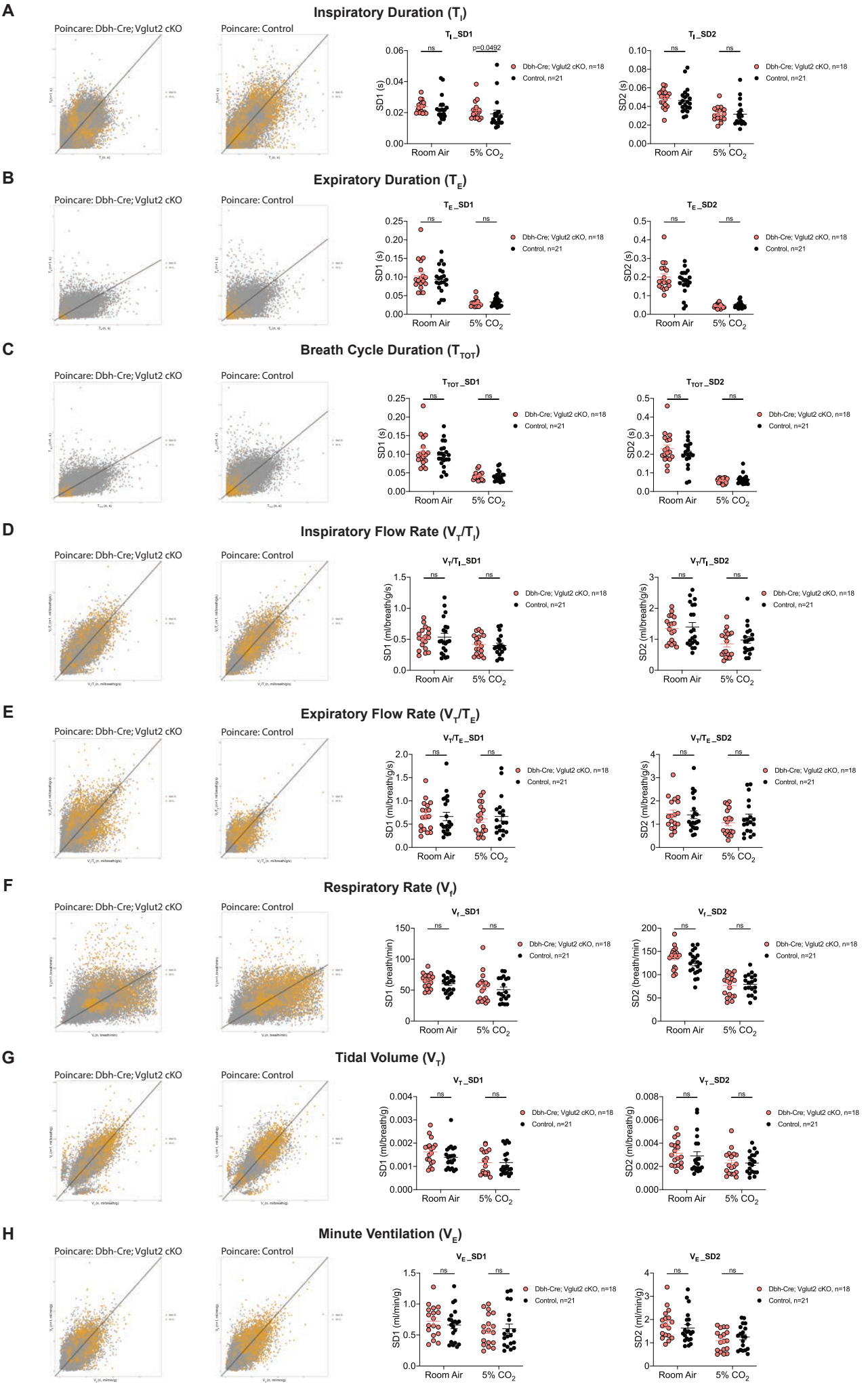

Figure 5 Supplement 1

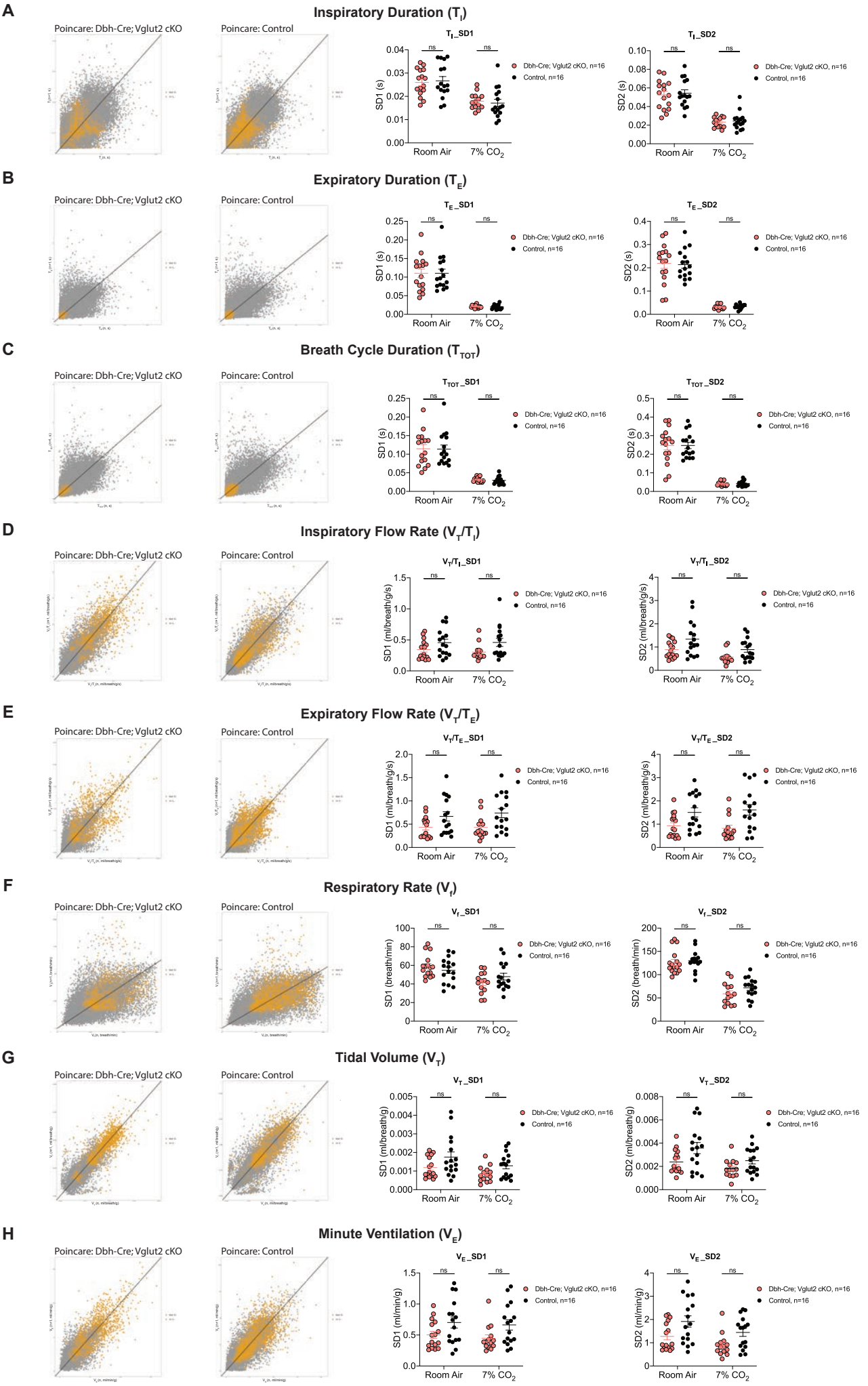

Figure 6 Supplement 1

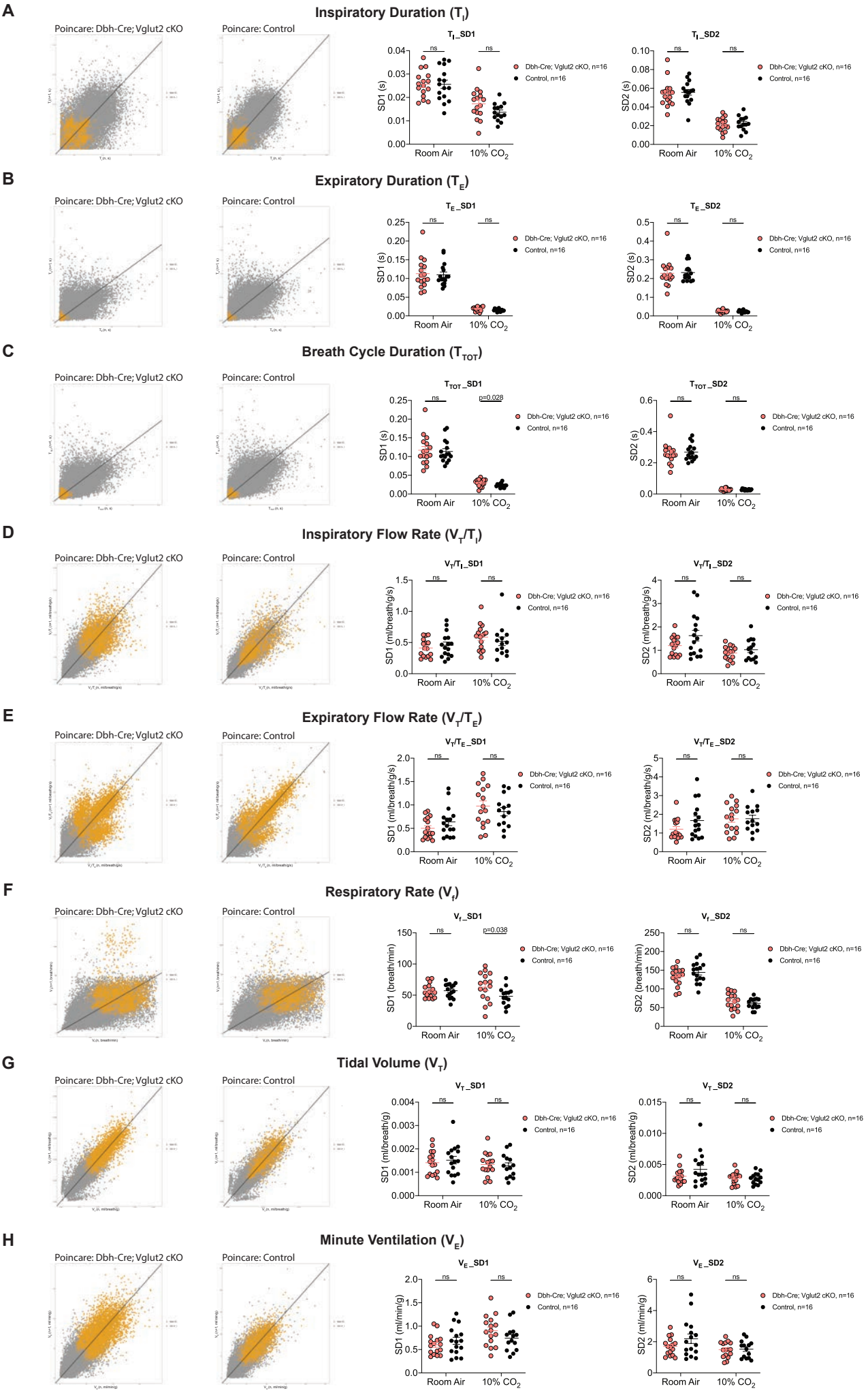

Figure 7 Supplement 1

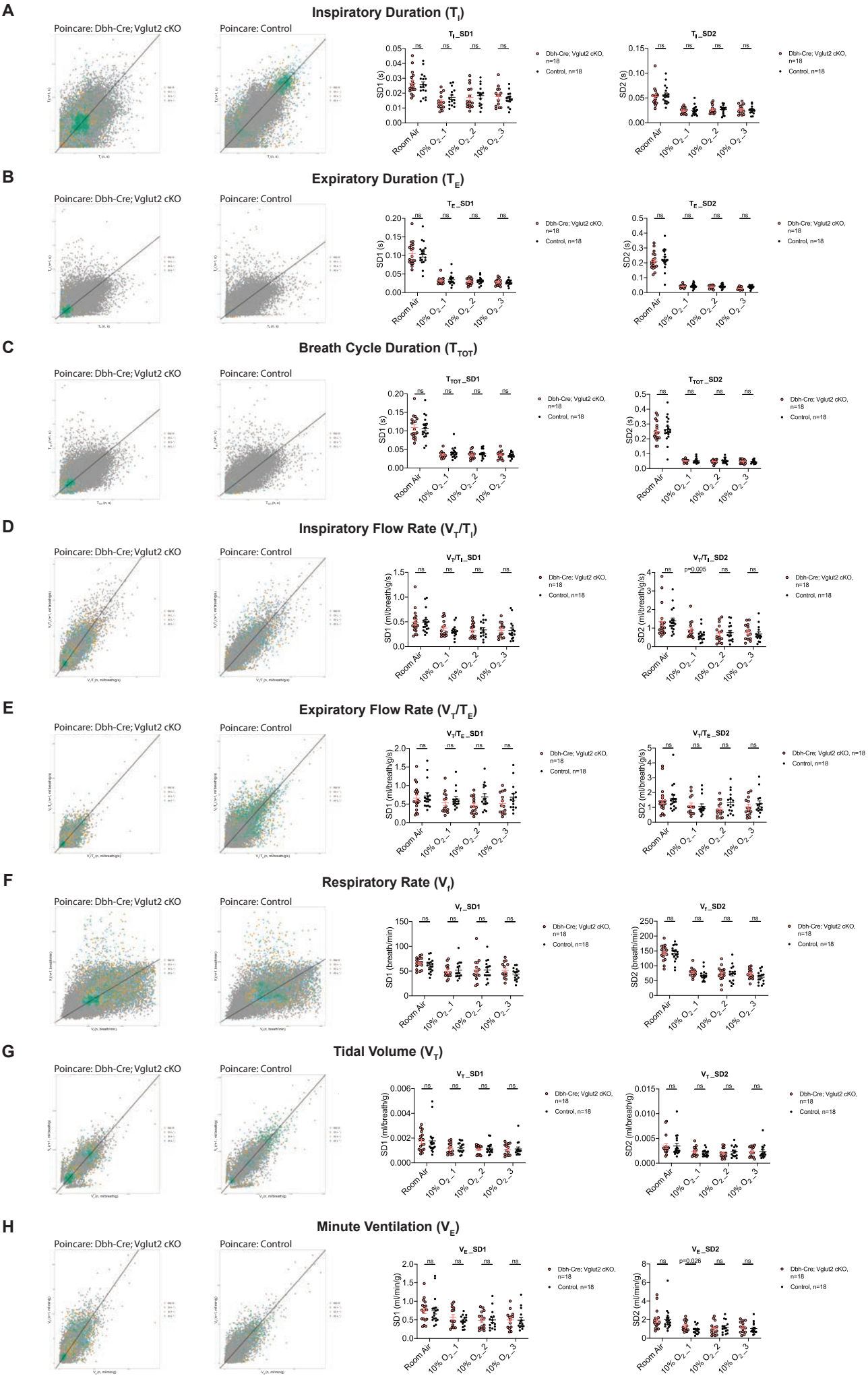

Table 1. Respiratory and metabolic values under room air conditions and the statistical tests

	Dbh-Cre; Vglut2 cKO Mean ± SEM	**Control Mean ± SEM**	**Dbh-Cre; Vglut2 cKO vs Control linear mixed-effects regression model**
V_E/V_{O2}	30.01 ± 2.58	33.22 ± 3.97	P = 0.98
V_f (Breaths/min)	204.08 ± 10.04	213.58 ± 15.36	P = 0.98
V_T (ml/Breath/g)	0.009 ± 0.0007	0.009 ± 0.0006	P = 0.88
V_E (ml/min/g)	1.93 ± 0.14	1.98 ± 0.22	P = 0.995
V_{O2} (ml/min/g)	0.067 ± 0.004	0.061 ± 0.004	P = 0.78
T_I (s)	0.117 ± 0.004	0.118 ± 0.005	P = 0.9999
T_E (s)	0.265 ± 0.020	0.255 ± 0.021	P = 0.996
T_{TOT} (s)	0.381 ± 0.022	0.373 ± 0.024	P = 0.99997
V_T/T_I (ml/Breath/g/s)	2.12 ± 0.16	2.33 ± 0.26	P = 0.996
V_T/T_E (ml/Breath/g/s)	1.43 ± 0.19	1.85 ± 0.39	P = 0.99

Table 2. Respiratory and metabolic values under 5% CO_2 conditions and the statistical tests

	Dbh-Cre; Vglut2 cKO Mean ± SEM	**Control Mean ± SEM**	**Dbh-Cre; Vglut2 cKO vs Control linear mixed-effects regression model**
V_E/V_{O2}	47.99 ± 3.28	58.60 ± 5.44	P = 0.33
V_f (Breaths/min)	246.72 ± 9.78	261.66 ± 14.00	P = 0.24
V_T (ml/Breath/g)	0.011 ± 0.0007	0.010 ± 0.0008	P = 0.81
V_E (ml/min/g)	2.67 ± 0.20	2.80 ± 0.32	P = 0.98
V_{O2} (ml/min/g)	0.057 ± 0.003	0.051 ± 0.005	P = 0.42
T_I (s)	0.119 ± 0.004	0.118 ± 0.007	P = 0.62
T_E (s)	0.135 ± 0.005	0.136 ± 0.007	P = 0.42
T_{TOT} (s)	0.255 ± 0.009	0.254 ± 0.013	P = 0.32
V_T/T_I (ml/Breath/g/s)	2.32 ± 0.21	2.45 ± 0.25	P = 0.99
V_T/T_E (ml/Breath/g/s)	2.17 ± 0.21	2.27 ± 0.25	P = 0.91

Table 3. Respiratory and metabolic values under 7% CO_2 conditions and the statistical tests

	Dbh-Cre; Vglut2 cKO Mean ± SEM	**Control Mean ± SEM**	**Dbh-Cre; Vglut2 cKO vs Control linear mixed-effects regression model**
V_E/V_{O2}	58.48 ± 4.29	74.70 ± 6.22	P = 0.23
V_f (Breaths/min)	262.69 ± 12.82	284.44 ± 10.59	P = 0.98
V_T (ml/Breath/g)	0.011 ± 0.0011	0.015 ± 0.0012	P = 0.023*
V_E (ml/min/g)	2.90 ± 0.32	4.23 ± 0.43	P = 0.16
V_{O2} (ml/min/g)	0.051 ± 0.004	0.059 ± 0.006	P = 0.64
T_I (s)	0.114 ± 0.005	0.112 ± 0.007	P = 0.90
T_E (s)	0.128 ± 0.008	0.111 ± 0.005	P = 0.69
T_{TOT} (s)	0.242 ± 0.012	0.223 ± 0.009	P = 0.81
V_T/T_I (ml/Breath/g/s)	1.93 ± 0.22	2.96 ± 0.33	P = 0.0016**
V_T/T_E (ml/Breath/g/s)	1.86 ± 0.25	3.18 ± 0.41	P = 0.075

Table 4. Respiratory and metabolic values under 10% CO_2 conditions and the statistical tests

	Dbh-Cre; Vglut2 cKO Mean ± SEM	Control Mean ± SEM	Dbh-Cre; Vglut2 cKO vs Control linear mixed-effects regression model
V_E/V_{O2}	105.77 ± 10.80	105.69 ± 11.51	P = 0.9996
V_f (Breaths/min)	336.31 ± 5.26	336.38 ± 8.52	P = 0.9997
V_T (ml/Breath/g)	0.018 ± 0.0015	0.016 ± 0.0012	P = 0.98
V_E (ml/min/g)	5.94 ± 0.48	5.54 ± 0.45	P = 0.9996
V_{O2} (ml/min/g)	0.059 ± 0.003	0.058 ± 0.005	P = 0.9999999
T_I (s)	0.099 ± 0.003	0.103 ± 0.004	P = 0.97
T_E (s)	0.085 ± 0.004	0.081 ± 0.006	P = 0.63
T_{TOT} (s)	0.184 ± 0.003	0.184 ± 0.005	P = 0.995
V_T/T_I (ml/Breath/g/s)	3.62 ± 0.25	3.61 ± 0.34	P = 0.9995
V_T/T_E (ml/Breath/g/s)	4.59 ± 0.39	5.06 ± 0.65	P = 0.86

Table 5. Respiratory and metabolic values under 10% O_2 conditions and the statistical tests

	Dbh-Cre; Vglut2 cKO Mean ± SEM	Control Mean ± SEM	Linear mixed-effects regression model	Dbh-Cre; Vglut2 cKO Mean ± SEM	Control Mean ± SEM	Linear mixed-effects regression model	Dbh-Cre; Vglut2 cKO Mean ± SEM	Control Mean ± SEM	Linear mixed-effects regression model
	10% O_2_1			10% O_2_2			10% O_2_3		
V_E/V_{O2}	43.79 ± 4.57	57.75 ± 10.88	P = 0.99	41.30 ± 3.85	49.36 ± 6.93	P = 0.99	42.82 ± 3.97	49.19 ± 6.02	P = 0.99
V_f (Breaths/min)	269.71 ± 8.49	243.89 ± 7.64	P = 0.67	268.38 ± 8.40	251.15 ± 8.67	P = 0.83	273.96 ± 9.31	255.84 ± 12.19	P = 0.80
V_T (ml/Breath/g)	0.009 ± 0.0009	0.010 ± 0.0009	P = 0.89	0.009 ± 0.0008	0.011 ± 0.0009	P = 0.85	0.009 ± 0.0009	0.011 ± 0.0013	P = 0.64
V_E (ml/min/g)	2.58 ± 0.25	2.40 ± 0.21	P = 0.999998	2.45 ± 0.24	2.65 ± 0.21	P = 0.9998	2.53 ± 0.24	2.92 ± 0.41	P = 0.998
V_{O2} (ml/min/g)	0.063 ± 0.008	0.055 ± 0.006	P = 0.995	0.063 ± 0.007	0.061 ± 0.005	P = 0.9998	0.064 ± 0.008	0.063 ± 0.006	P = 0.99999999
T_I (s)	0.111 ± 0.005	0.126 ± 0.010	P = 0.44	0.115 ± 0.006	0.131 ± 0.012	P = 0.51	0.116 ± 0.006	0.132 ± 0.011	P = 0.44
T_E (s)	0.123 ± 0.007	0.133 ± 0.009	P = 0.995	0.119 ± 0.006	0.121 ± 0.008	P = 0.9999	0.114 ± 0.007	0.117 ± 0.008	P = 0.9997
T_{TOT} (s)	0.234 ± 0.007	0.259 ± 0.009	P = 0.53	0.234 ± 0.007	0.252 ± 0.009	P = 0.75	0.230 ± 0.008	0.248 ± 0.011	P = 0.69
V_T/T_I (ml/Breath/g/s)	1.83 ± 0.23	1.83 ± 0.20	P = 0.9999	1.66 ± 0.19	1.91 ± 0.20	P = 0.998	1.67 ± 0.18	1.98 ± 0.26	P = 0.99
V_T/T_E (ml/Breath/g/s)	1.79 ± 0.24	2.00 ± 0.29	P = 0.9994	1.69 ± 0.21	2.32 ± 0.32	P =0.99	1.83 ± 0.21	2.67 ± 0.51	P = 0.98

Supplemental table 1. Vglut2 positive innervations from central noradrenergic neurons to the brain nuclei important in breathing control

Vglut2$^+$ noradrenergic nuclei	Downstream target of Vglut2$^+$ NA neurons	The role of the downstream target in breathing control	Reference
C1	preBötzinger complex	Generate inspiratory rhythm	Malheiros-Lima et al. (2018)
	parafacial region (pFRG)	Regulate active expiration during chemosensory stimulation	Malheiros-Lima et al. (2020)
	Locus Coeruleus (LC)	Chemosensitive, regulate chemosensation	Abbott et al. (2013); Holloway et al. (2013)
	A5	Inhibitory drive for chemosensation and respiratory rhythm	Abbott et al. (2013); Malheiros-Lima et al. (2022)
	A1, A2	Modulate chemosensation, stabilize respiratory rhythm	Abbott et al. (2013); Holloway et al. (2013)
	Lateral parabrachial nucleus (PBN)	Regulate chemosensation and arousal	Abbott et al. (2013)
	Medullary raphe	Regulate chemosensation and expiration	Abbott et al. (2013)
	Nucleus of the solitary tract (NTS)	Receive input from the carotid bodies (a key center for O_2 chemosensation) and other cardiopulmonary afferents	Abbott et al. (2013)
	Dorsal motor nucleus of the vagus	Control respiration rate, regulate airway tone and defense	Abbott et al. (2013)
	Dorsomedial hypothalamus (DMH) lateral hypothalamic area (LHA)	Modulate baseline respiration, chemosensation, arousal	Abbott et al. (2013)
	Paraventricular thalamic nucleus (PVT)	Regulate arousal	Abbott et al. (2013)
	Paraventricular nucleus (PVN)	Modulate baseline respiration, respiratory response to hypoxia	Abbott et al. (2013)
Locus Coeruleus (LC)	Lateral parabrachial nucleus	Regulate chemosensation and arousal	Yang et al. (2021)